Reaction Chemistry & Engineering

ROYAL SOCIETY OF CHEMISTRY

PAPER

View Article Online
View Journal | View Issue

Cite this: *React. Chem. Eng.*, 2024, **9**, 1666

Selective catalytic oxidation of humins to carboxylic acids using the $H_4[PVMo_{11}O_{40}]$ Keggin-type polyoxometalate enhanced by alcohol doping and solubilizer†

Tobias Esser, André Wassenberg, Dorothea Voß and Jakob Albert *

Oxidative valorization of humins is one promising approach for establishing carbon efficient biomass valorization pathways. In the present contribution, the development of an optimized reaction system for the selective catalytic oxidation (SCO) of water-insoluble and highly complex humins to short-chain carboxylic acids like formic acid (FA) and acetic acid (AA) using Keggin-type polyoxometalates is presented. In detail, the monovanadium-substituted polyoxometalate $H_4[PVMo_{11}O_{40}]$ catalyst exhibited a considerable selectivity advantage in the aqueous phase over state-of-the-art catalysts. More specifically, the yield of the desired products FA and AA (esters) could be drastically improved up to 30%, while undesired side products resulting from thermal-induced decarbonylation and decarboxylation were drastically reduced down to a third. Hereby, alcoholic additives like methanol show a remarkable inhibiting effect on CO_2 formation. It was shown that a temperature of 120 °C represents an optimum where methanol can still inhibit CO_2 formation even at a low alcohol content of 5 vol%. Furthermore, the use of *para*-toluenesulfonic acid (*p*TSA) as solubilizer has been investigated to circumvent the water-insoluble character of humins and to optimize humin conversion. On the one hand, *p*TSA could efficiently promote the activity in the SCO of humins. On the other hand, methanol was far more efficient in inhibiting CO_2 formation, especially at elevated reaction temperatures. The results were reproducible and could even be transferred to various humins based on different sugars. Using the combination of methanol and *p*TSA as additives as well as a singly vanadium-substituted polyoxometalate catalyst provides a highly promising approach for the valorization of complex humins.

Received 12th December 2023,
Accepted 5th March 2024

DOI: 10.1039/d3re00672g

rsc.li/reaction-engineering

In recent years, the industrial valorization of biomass to produce platform chemicals such as levulinic acid has increasingly grown in importance.[1–5] The driving force behind this development is the increasing demand for energy and chemicals as well as the depletion of fossil hydrocarbon sources. However, only a few bio-based process technologies have been able to establish themselves in industry so far, as they are often more demanding and complex.[6–8] One deficit is the formation of undesirable by-products by thermal-induced reactions that make such processes inefficient and expensive.[9,10] In this context, the Biofine process for the acid-catalyzed production of biogenic levulinic acid is one example.[11,12] In this process, insoluble black polymeric solids are formed as by-products, the so-called humins.[5,13,14] Humins are a typical by-product of acid-catalyzed conversion of carbohydrates, decreasing the overall carbon efficiency of such processes.[9,10,15]

The formation and structure of humins have received much attention in recent years. The humin structure is built by a furan-rich polymer network.[16] Linkage of these furan rings can take place *via* either oxygen functionalized C–O–C bonds or aliphatic C–C bonds.[17,18] However, there are still controversial discussions about the complex structure of humins that has not been fully elucidated to date.

Several approaches were pursued to suppress the formation of humins in the acid-catalyzed conversion of carbohydrates. However, these approaches fail due to the fast kinetics of humin formation.[5,14,19,20] Another promising idea is the chemical valorization of humins by catalytic oxidation.[5,21] Pioneering work in this field was done by Maerten *et al.*,[5] who demonstrated for the first time the chemical valorization of humins by selective catalytic

Institute of Technical and Macromolecular Chemistry, Universität Hamburg, Bundesstraße 45, 20146 Hamburg, Germany.
E-mail: jakob.albert@uni-hamburg.de; Tel: (+49) 4042838 4209

† Electronic supplementary information (ESI) available: Various additional results and analytical data of reaction solutions. See DOI: https://doi.org/10.1039/d3re00672g

oxidation (SCO) using polyoxometalate (POM) catalysts to short-chain carboxylic acids. POMs are a unique class of inorganic compounds having a wide variety of geometric and electronic structural properties. Moreover, they are ideal prototypes for catalytic applications as they combine the required reactivity and stability at the molecular level.[22] More specifically, the study of Maerten *et al.*[5] showed that a five times vanadium-substituted Keggin-type phosphomolybdic acid $H_8[PV_5Mo_7O_{40}]$ (HPA-5) catalyst could promote humin conversion up to about 89% under very mild conditions of 120 °C and 20 bar oxygen pressure in pure aqueous medium within one hour of reaction time. Unfortunately, CO_2 was the main reaction product with up to 80% yield.[5] Lowering the reaction temperature down to 90 °C lowers conversion but prevents thermal-induced total oxidation to CO_2 to a certain extent and therefore increased the selectivity of value-added products up to 11% for formic acid (FA) and 5% for acetic acid (AA).[5] However, only a small fraction of the carbon provided by humins was converted into value-added products, which is so far a major obstacle for catalytic oxidative valorization approaches. Further results published by Wassenberg *et al.*,[21] where various sugar-derived humins were oxidized in the aqueous phase using HPA-5 showed interesting correlations between humin structure and conversion, showing that ether and ester groups were converted very well by catalytic oxidation, while thioester and ether groups were only poorly oxidized. The furan-containing core structure of the humins remained mostly unaffected by the oxidative treatment. In both studies, humins from different carbohydrates like glucose, fructose or cellobiose were efficiently converted and short-chain carboxylic acids were successfully obtained as value-added products. However, the results showed that vanadium-substituted Keggin-type POMs can be used to oxidize very complex aromatic structures like humins to carboxylic acids. Inspired by the aforementioned results, Esser *et al.*[23] used individual monofuran derivatives like 5-hydroxymethylfurfural (HMF), furfural, 2-furoic acid, 2(5*H*)-furanone, 2-furfuryl alcohol and 2-methylfuran to gain a deeper understanding of POM-catalyzed humin oxidation. Hereby, they found that the Keggin-type POM-catalyst $H_4[PVMo_{11}O_{40}]$ (HPA-1) can oxidize both monofuran and difuran derivatives or even branched furan rings to maleic acid (MA) and FA, respectively. It was shown that oxygen-functionalized bond types can be converted much better than non-functionalized C–C bonds. The use of more highly V-substituted POMs improved the oxidation of the C–C bonds. However, the MA-yield decreased with an increasing degree of V-substitution, while both FA yield and over-oxidation to CO_2 increased.

Therefore, the main scope of the present study was the optimization of this promising approach for real humin structures. In detail, the use of solubilizers like *para*-toluene sulfonic acid (*p*TSA) and short-chain alcohols as co-solvents in combination with different reaction temperatures on both the kinetics and the selectivity of HPA-1-catalyzed SCO of humins was studied.

Results and discussion

SCO of humins using vanadium-substituted POM catalysts

As results in the literature have shown, vanadium-substituted POM catalysts exhibit remarkable activity in the SCO of complex biomass, including humins.[5,21,24] In particular, vanadium-substituted phosphomolybdic acid, which forms Keggin-type POM catalysts, proves to be an active catalyst for the oxidative conversion of biomass in aqueous medium. It is plausible that peroxo-ligands located between adjacent vanadium atoms in higher vanadium-substituted POMs are responsible for the enhanced activity, as reported by Poller *et al.*[25] In particular, in the SCO of humins, this high activity of catalytic species leads to over-oxidation and thus to increased CO_2 formation.[5,21]

Analogous findings could be demonstrated by previously published results on the oxidation of mono-furan derivatives and humin-like substances.[23] Here, higher substituted POMs showed significant higher activity for the oxidation of the mono-furan derivative furfural, which was ultimately converted to formic acid (FA) or to CO_2 with yields up to 43% and 30%, respectively. In comparison, the $H_4[PVMo_{11}O_{40}]$ (HPA-1) catalyst was characterized by a much lower tendency to over-oxidation with CO_2 yields of only around 5%. In addition, maleic acid (MA) could be produced as one of the main products with a yield of up to 22%, while higher vanadium-substituted catalysts further degraded the carbon skeleton to FA and CO_2.

Due to the lower tendency of the HPA-1 catalyst to over-oxidize the carbon skeleton to CO_2 and the resulting selectivity advantage, it was applied for the first time in the SCO of real humins. The substrate used was a glucose-based humin prepared by the acid-catalyzed synthesis of levulinic acid from glucose. The detailed experimental procedure can be found in the corresponding section of the experimental part. Humins are very complex substrates whose structure has not yet been clearly clarified. Various investigations employing diverse analytical methods have been carried out in the past few years to further clarify the humin structure.[5,9,15,19,20] According to these analyses, numerous studies describe the humin structure as a furan-rich polymer network that is cross-linked *via* both oxygen-functionalized and aliphatic bonds without oxygen.[4,5,9,16–18,21,26–29] Fig. 1 shows the spectra obtained by Fourier-transform infrared spectroscopy (FTIR) of the glucose-based humin used and the glucose used to produce it. The fundamental frequencies of glucose are caused by the stretching of the hydroxyl groups at about 3300 cm^{-1}, in the range of 2950 cm^{-1} to 2890 cm^{-1} by the aliphatic C–H stretching and by the deformation of the C–O–C and C–O–H bonds at 1460 cm^{-1} to 1340 cm^{-1}. In the range of approx. 1150 cm^{-1} to 990 cm^{-1}, carbohydrate-characteristic vibrations of C–O and C–C can be found. Compared to the spectrum of glucose, the vibrations of the hydroxyl groups are absent, and two new humin-typical signals were detected at around 1600 cm^{-1} and 1700 cm^{-1}. These signals could be assigned to the C=C stretching

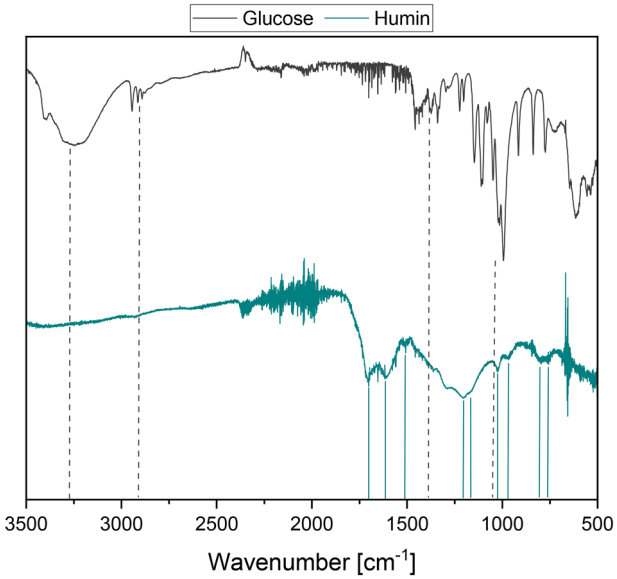

Fig. 1 FTIR spectra of glucose (top, gray) and glucose-based humin (bottom, turquoise).

vibration conjugated with carbonyl at 1600 cm^{-1} and the C═O stretching vibration at 1700 cm^{-1}.[21,30] The described development of the signals is consistent with the formation mechanisms of humins postulated in the literature.[16,17,21,30,31] Accordingly, glucose dehydrates under acid catalysis in the first step to 5-hydroxymethylfurfural (5-HMF), which reacts further to obtain levulinic acid (LeA) under ring opening. In the studies by Wassenberg *et al.*,[21] both intermediates were detected as part of the liquid reaction phase of the acid-catalyzed conversion of hexoses. 2,5-Dioxo-6-hydroxyhexanal (DHH) is also discussed as a possible intermediate, but it has not yet been proven experimentally.[15,32]

These highly functional molecules can react further in various ways, *e.g.* by aldol condensation. In this process, the hydroxyl groups of glucose were completely converted, while C═C and C═O bonds were formed. Continuing cross-linking can take place through etherification, esterification, acetylation, and further aldol condensations. Shen *et al.*[17] provide a comprehensive overview of reactions and mechanisms involved in the formation of humins. Other characteristic vibrations that indicate the furan-rich network are the C═C stretching vibration of the polysubstituted furans at around 1500 cm^{-1}, the C–O–C deformation of the furan rings at around 1160 cm^{-1} and 1200 cm^{-1} and the C–H vibrations at around 965 cm^{-1}, 800 cm^{-1} and 760 cm^{-1}. A number of structural elements and possible humin structures can be derived from the bonding types and basic building blocks described. Wassenberg *et al.*[21] provide experimentally proven structural elements of humins in their study. A comprehensive overview of further structural motifs of humins can be found in the review by Liu *et al.*[9] Furthermore, a detailed discussion of various structural elements, important functional groups and possible humin-like model substances with regard to a catalytic conversion of humins can be found in previously published results.[23]

The morphology of the humin used could also be of interest. For this purpose, the humin produced was examined using scanning electron microscopy (SEM). The results of SEM analysis can be found in Fig. 2. Under traditional conditions, humins mostly consist of agglomerated spherical particles. These interconnected spheres can also be found for the used glucose-based humin (Fig. 2). It can be assumed that the increased participation of LeA in the poly-furanic network presumably prevents the highly ordered stacking orientation by causing more aldol condensations and concurrently esterification.[17] This results in a coexistence of more agglomerated particles with a less layered structure.[17] Due to the high reaction rate at 180 °C, larger clusters were preferably formed.

Table 1 shows the results of the SCO of humin using the HPA-1 catalyst in comparison to higher substituted HPA-2 and HPA-5 as well as a Lindqvist-type $K_5[PV_3W_3O_{19}]$ (IPA-3) POM-catalyst. The results using the HPA-5 and IPA-3 catalysts were published by Maerten *et al.*[5] and serve to supplement or support the trends identified here. As a reference, an experiment without catalyst (blank) was also carried out in pure aqueous phase. The liquid samples were analyzed by one-dimensional nuclear magnetic resonance (NMR) spectroscopy and the gaseous samples by gas chromatography (GC). The exact procedure can be found in the corresponding section of the experimental part. Furthermore, for the liquid product phase, two-dimensional NMR measurements such as heteronuclear single quantum coherence (HSQC) and heteronuclear multiple bond correlation (HMBC) were performed to exactly reveal the formed structures. Example spectra for the 1D NMR measurements of nuclei ^{1}H as well as ^{13}C and for the 2D NMR measurements HSQC and HMBC can be found in the ESI† (Fig. S1–S4). In addition, all results could be confirmed by high-,performance liquid chromatography (HPLC) measurements summarized in Table S1.†

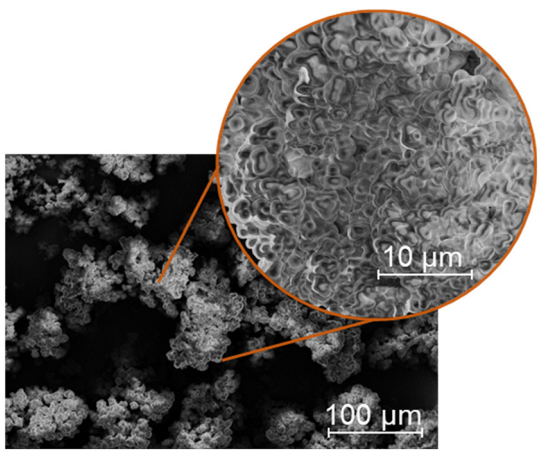

Fig. 2 SEM image of glucose-based humin.

Table 1 Selective catalytic oxidation of humins using different POM catalysts

Entry	Catalyst	Total yield/%	Combined yield/%		Ratio[e] (value : waste)/%
			FA + AA[c]	CO + CO_2[d]	
1[a]	Blank	11.2	3.2	8.0	29 : 71
2[a]	HPA-1	30.1	10.9	19.2	36 : 64
3[a]	HPA-2	56.3	7.3	49.1	13 : 87
4[b]	IPA-3	69.9	11.3	58.6	16 : 84
5[b]	HPA-5	77.1	12.3	64.8	16 : 84

Experimental conditions: [a] 3-Fold reaction system, 90 °C, 30 bar O_2, 30 h, 1000 rpm, 300 mg solid humin (16.2 mmol carbon), 0.83 mmol of vanadium (V) for substitution (20 mol_{Carbon} mol_V^{-1}) in 30 mL water. [b] Results of Maerten *et al.*[5] [c] Determined with quantitative ^1H NMR and *tert*-butanol as standard. [d] Determined with GC-TCD. [e] Calculated as described in the corresponding section of the experimental part.

Without the use of a catalyst, the complex humin could hardly be converted, with a total yield of about 11% (Table 1, entry 1). In the gas phase, CO_2 was formed as the main product with a yield of over 7%. FA and AA, which were formed as liquid phase products, were present in approximately equal amounts with yields of 1.5% and 1.8%, respectively.

The combined yield of the gas phase products CO and CO_2 was about 8%, which is 2.5 times higher than the combined yield of the carboxylic acids FA and AA, which was only about 3%. Therefore, the ratio of the value-added products FA as well as AA (value) and the undesired gas-phase products (waste) has reached 29 : 71. As expected, the use of the HPA-1 catalyst results in a drastic increase in activity, tripling the total yield to over 30% (Table 1, entry 2). The combined yield of the value-added products FA and AA was also increased to almost 11%. Due to the use of the redox-active HPA-1 catalyst, the combined yield of gas phase products increased only up to a value of about 19%. Thereby, the ratio of value-added products to waste slightly improves to 36 : 64. It can be concluded that the use of the HPA-1 catalyst significantly increases the activity in the SCO of humins but has only a minor effect on the selectivity compared to the uncatalyzed reaction.

As already described, higher vanadium-substituted POM catalysts exhibit increased catalytic activity due to the formation of peroxo-species.[23,25] Consequently, the use of the double-substituted HPA-2 catalyst led to a fivefold increase in the total yield to about 56% compared to the reaction without catalyst (Table 1, entry 3). Compared to that of the reaction catalyzed by HPA-1, the total yield increased by a factor of more than 2. This confirms the expected increase in activity due to a higher degree of substitution. Considering the results of Maerten *et al.*,[5] an increase in catalytic activity with increasing degree of substitution could also be observed (Table 1, entries 4 and 5). The total yield increased to about 70% and over 77% using IPA-3 or HPA-5, respectively. According to the results, the application of higher substituted POM catalysts is beneficial concerning the activity. However, the use of a singly vanadium-substituted POM already decreased the formation of CO_2 compared to the results using higher vanadium-substituted catalysts (Table 1, entries 3 and 4). More specifically, the use of the five times vanadium-substituted HPA-5 resulted in 65% yield of undesired gas-phase products, which is more than three times higher compared to the results using HPA-1.[5] Moreover, a combined yield of carboxylic acids of about 12% was obtained, which is only slightly more than the results presented here.[5] Therefore, the use of the HPA-5 catalyst only allows for a considerably less favorable ratio of value-added products and undesired by-products of 16 : 84. The use of the triple-substituted Lindqvist-type IPA-3 also led to increased CO_2 formation (Table 1, entry 4).[5] Accordingly, higher vanadium-substituted POM catalysts are much more active, but also promote the overoxidation of humins to CO_2. The tendency of higher substituted POM catalysts to overoxidize the substrate is a well-known and well-studied phenomenon in the literature, yielding CO_2 as the main product.[33–36] Consequently, the use of HPA-1 as a catalyst is beneficial concerning the selectivity to short-chain carboxylic acids, which is crucial for a sustainable valorization of humins. Nevertheless, CO_2, whose yields were at least twice that of the value-added products, is the main product in the SCO of humins, regardless of the catalyst used. Hence, it seems reasonable to investigate additional features that can suppress or inhibit CO_2 formation in the SCO of humins. To this end, short-chain alcohols have been discussed in the literature as additives that demonstrated remarkable results in inhibiting CO_2 formation during oxidative conversion of biomass.[35–37] Short-chain alcohols such as methanol (MeOH) or ethanol (EtOH) succeeded in optimizing oxidation reactions and inhibiting formation of CO_2 using vanadium-based catalysts by acting as radical scavengers, stabilizing reactive groups of substrates and forming new catalytic species as well as increasing the solubility of oxygen.[33–37] The transferability of these remarkable effects to the SCO of humins using HPA-1 as a catalyst needs to be further investigated.

Selection of a suitable additive for the suppression of CO_2 formation in the SCO of humins

The suppression of CO_2 formation during the oxidative valorization of biomass by using short-chain alcohols as additives represents a promising approach. Remarkable results have been achieved, especially when methanol was

used.[34,35,37] Maerten *et al.*[35] demonstrated the oxidation of glucose to FA and its ester methyl formate (MF) in nearly perfect selectivity by outstanding CO_2 suppression using methanol as a (co)-solvent. It was reported that the selectivity of FA using glucose as a substrate in an aqueous-methanolic solvent system could be increased from about 50% to over 99% catalyzed by HPA-5.[35] Hereby, the undesirable over-oxidation of the substrate to CO_2 was efficiently prevented. Furthermore, it was shown that even a low alcohol content of 10 vol% methanol in aqueous solution allowed for a significant improvement in the yield of carboxylic acids and a very effective suppression of the formation of gaseous by-products.[35] Similar results were also obtained by He *et al.*[36] and Lu *et al.*[34] in their studies. Lu *et al.*[34] demonstrated the inhibition of CO_2 formation in oxidative conversion of glucose to FA using $H_5[PV_2Mo_{10}O_{40}]$ (HPA-2) as a catalyst by decreasing the CO_2 yield from about 45% in pure water to less than 4%, even at a low methanol content of at least 10 vol%.

Based on the aforementioned promising results in the oxidative conversion of glucose from the literature, the transferability to the SCO of humins using HPA-1 as a catalyst was further investigated. For this purpose, the SCO of glucose-based humin was studied using an aqueous solution of 10 vol% methanol. In addition, ethanol and isopropanol (iPrOH) were tested as further alcohol additives. For all additives, a stability test was also performed without a substrate under otherwise identical conditions to demonstrate that the carboxylic acids originated only from the carbon in the substrate and not of the organic additive. The results are shown in Table 2.

According to the results shown in Table 2, addition of 10 vol% methanol as an additive led to a significant decrease in yield of the undesired side products CO and CO_2 from above 19% to below 12% compared to a purely aqueous system (Table 2, entries 1 and 2). In an aqueous-alcohol solution, carboxylic acids are partly present as esters, which are formed by esterification with the corresponding alcohol. Due to the low alcohol content and the associated excess water, the equilibrium is on the side of the hydrolysis products. The yield of carboxylic acids (esters) also increased from under 11% to about 14%. The use of a 10 vol% ethanolic solution also led to a visible inhibition of the formation of gaseous by-products with a yield of about 14% (Table 2, entry 3). Analogously to methanol, the yield of carboxylic acids slightly increased to about 14%. Thus, the ratio of value-added products (carboxylic acids and esters) to undesired by-products (CO/CO_2) was 50 : 50 and 54 : 46 when using an ethanolic solution or a methanolic solution, respectively (Table 2, entries 2 and 3). Therefore, addition of methanol is more efficient than addition of ethanol. In this way, the complex humin was converted into more value-added products than into undesired by-products. This is an impressive increase over the reaction without alcohol addition, where the yield of undesired by-products was at least twice that of the value-added products. Addition of isopropanol also showed CO_2-inhibiting effects, but these are less pronounced than that with addition of methanol (Table 2, entry 4).

To exclude formation of carboxylic acids or their esters from alcohols under the reaction conditions, additional experiments without a substrate were conducted. The liquid phase of each experiment was analyzed by NMR and HPLC. The NMR spectra and chromatograms can be found in the ESI (Fig. S5 and S6†). It was found that without a substrate no carboxylic acids or esters were formed, confirming the sole origin of FA, MF and AA from the substrate (Table 2, entries 5–7). Comparable results were published by Maerten *et al.*[35] and further verified by labeling experiments with ^{13}C-labeled glucose. Also, Lu *et al.*[34] have investigated the formation of carboxylic acids and esters originated from additives using deuterated alcohols. All detected FA was not D-labeled and thus formed from the substrate.[34]

Effect of MeOH concentration and reaction temperature on the SCO of humins

It has been shown that an addition of 10 vol% methanol already inhibits the formation of CO_2 in the SCO of humins using HPA-1 as a catalyst. However, the influence of

Table 2 SCO of glucose-based humin using HPA-1 as catalyst in aqueous media with 10 vol% alcohol additive

Entry[a]	Substrate	Additive	Total yield/%	Combined yield/%		Ratio[dd] (value : waste)/%
				FA + AA + esters[b]	CO + CO_2[c]	
1	Humin (Gl)	—	30.1	10.9	19.2	36 : 64
2	Humin (Gl)	MeOH	25.7	13.8	11.9	54 : 46
3	Humin (Gl)	EtOH	27.8	13.9	13.9	50 : 50
4	Humin (Gl)	iPrOH	24.6	10.7	13.9	44 : 57
5	—	MeOH	0.0	0.0	0.0	—
6	—	EtOH	0.0	0.0	0.0	—
7	—	iPrOH	0.0	0.0	0.0	—

Experimental conditions: [a] 3-Fold reaction system, 90 °C, 30 bar O_2, 30 h, 1000 rpm, 300 mg solid humin (16.2 mmol carbon), 0.83 mmol of vanadium (V) for substitution (20 mol_{Carbon} mol_V^{-1}) in 30 mL aqueous alcohol solution with 10 vol% of the respective alcohol. [b] Determined with quantitative ^1H NMR and *tert*-butanol as standard. [c] Determined with GC-TCD. [d] Calculated as described in the corresponding section of the experimental part.

Table 3 SCO of humin using HPA-1 as catalyst in an aqueous methanolic system with different amounts of methanol

Entry[a]	Catalyst	Amount of MeOH/%	Total yield/%	Combined yield/%		Ratio[d] (value : waste)/%
				FA + AA + esters[b]	CO + CO_2[c]	
1	HPA-1	5	27.2	14.7	12.5	54 : 46
2	HPA-1	10	25.7	13.8	11.9	54 : 46
3	HPA-1	20	26.1	12.8	13.4	49 : 51
4	Blank	5	8.6	3.4	5.2	40 : 60

Experimental conditions: [a] 3-Fold reaction system, 90 °C, 30 bar (O_2), 30 h, 1000 rpm, 300 mg solid humin (16.20 mmol carbon), 0.83 mmol of vanadium (V) for substitution (20 mol_{Carbon} mol_V^{-1}) in 30 mL aqueous alcohol solution with 0–20 vol% methanol. [b] Determined with quantitative ^{1}H NMR and *tert*-butanol as standard. [c] Determined with GC-TCD. [d] Calculated as described in the corresponding section of the experimental part.

methanol content on the inhibition of CO_2 formation for this reaction system has not been investigated so far. For this purpose, further experiments were conducted by adding 5% and 20% methanol to the aqueous solution. The results are shown in Table 3.

According to the results shown in Table 3, the amount of methanol used in the studied range has no significant influence (entries 1–3) on the product selectivity. Concerning the ratio of value-added products to undesired side products, the addition of 5 vol% methanol did not differ from the base experiment with the addition of 10 vol% methanol. Interestingly, the lowest methanol content of 5 vol% enabled the highest combined yield of carboxylic acids of almost 15%, but at the same time the second lowest yield of undesired by-products of around 12% (Table 3, entry 1). Increasing the methanol content up to 20 vol% resulted in slightly lower performance. More specifically, the yield of carboxylic acids decreased to less than 13%, while the yield of gaseous products increased to over 13%. Therefore, further increasing the methanol content is considered inefficient. Furthermore, the methanol content influenced the yield of MF, which increased from 0.9% to 2.8% as the methanol content increased. The methanol content affects the equilibrium of the esterification reaction of FA. However, due to the excess of water and the resulting favored hydrolysis of esters, most of the products were free acids. For further experiments, a methanol content of 5 vol% was chosen because this content enabled the highest yield of carboxylic acids while efficiently inhibiting CO_2 formation. In addition, a lower methanol content is more cost-effective and would therefore have an advantage in a technical-economic system analysis.

The reference reaction without catalyst (blank) also demonstrated the effectiveness of adding 5 vol% methanol for inhibiting CO_2 formation (Table 3, entry 4). Still, the yield of carboxylic acids was more than four times higher when a catalyst was used. Nevertheless, the total yield of about 27% including the combined yield of carboxylic acids of about 15% is still low (Table 3, entry 1). In order to increase the yield of carboxylic acids, experiments were conducted at different reaction temperatures and the influence on the kinetics of the reaction was investigated. The results are shown in Fig. 3. As expected, a strong increase in the activity was achieved as the reaction temperature increased. The total yield drastically increased from about 27% to over 60% at reaction temperatures of 90 °C and 130 °C, respectively. The highest yield of carboxylic acids of about 29% was achieved at 120 °C, which is almost twice the yield at 90 °C. Increasing the temperature further up to 130 °C, the yield of carboxylic acids remains almost unchanged. Interestingly, the yield of undesired by-products increased from under 29% at 120 °C to about 33% at 130 °C. Consequently, the ratio of value-added products to undesirable by-products shifted in favor of the by-products, resulting in more CO_2 being formed than carboxylic acids. In the temperature range from 90 °C to 120 °C, the combined yields of carboxylic acids and undesirable by-products increased to approximately the same extent with increasing temperature. Hence, the ratio of value-added products to undesirable by-products changed only slightly from 54 : 46 to 50 : 50 in the temperature range between 90 °C and 120 °C. Overall, a reaction temperature of 120 °C is the most efficient concerning the increase in yield of carboxylic

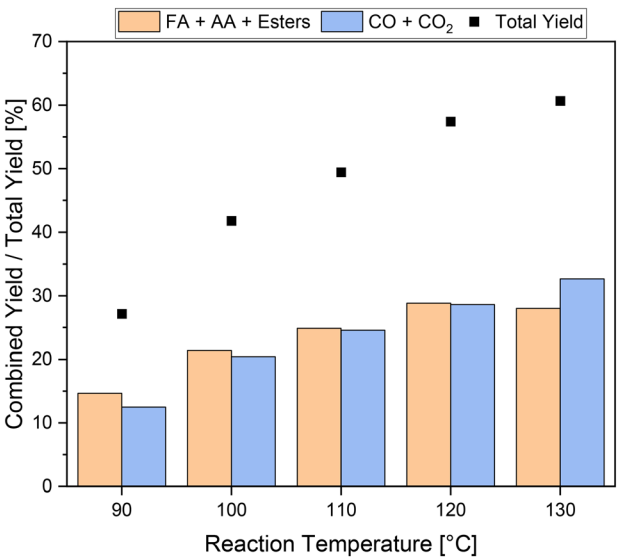

Fig. 3 SCO of humins using HPA-1 as a catalyst at different reaction temperatures in aqueous-methanolic solution. Experimental conditions: 3-fold reaction system, 90–120 °C, 30 bar O_2, 30 h, 1000 rpm, 300 mg solid humin (16.2 mmol carbon), 0.83 mmol of vanadium (V) for substitution (20 mol_{Carbon} mol_V^{-1}) in 5 vol% methanol.

acids and still effective inhibition of CO_2 formation. The stability test with methanol without substrate showed no formation of carboxylic acids up to a reaction temperature of 130 °C, confirming that the value-added products still originated from the humin substrate.

Effect of *p*TSA as solubilizer on the SCO of humins

It is well known that humins are virtually insoluble in commonly known solvents.[5,21,29] The low solubility of humins hampers their chemical valorization in the liquid phase. In the literature, the use of solubilizers in the oxidative processing of biogenic raw materials and complex biomass is discussed.[38] *para*-Toluene sulfonic acid (*p*TSA) has proven to be one of the most promising solubilizers.[38–44]

The application of *p*TSA for *in situ* solubilization of the substrate and enhancement of activity in the SCO of humins was further investigated. To this end, the oxidation of glucose-based humin was studied using 3 mmol *p*TSA as solubilizer under the initial reaction conditions (90 °C) in aqueous medium. First, the addition of methanol was deliberately avoided in order to be able to assess the influence of *p*TSA as a solubilizer. For the same purpose, the reaction temperature was reset to 90 °C, which also allowed separate consideration of temperature effects on this reaction system. As reference, an experiment was conducted without a catalyst but with the addition of *p*TSA. The results are displayed in Table 4. In the purely thermal reaction without a catalyst, the use of *p*TSA had only a small influence on the activity, with an increase in total yield from about 11% to about 14% compared to the reaction without *p*TSA (Table 4, entries 1 and 2). Interestingly, the combined yield of CO and CO_2 was hardly influenced between these two reactions. However, a combined yield of carboxylic acids of over 7% could be achieved with a combined yield of CO and CO_2 of only 7%, which is almost twice as high as in the reaction without *p*TSA.

It seems evident that the use of *p*TSA resulted in more easily converted humin fragments, which in turn were oxidized into FA and AA. The addition of *p*TSA in the reaction catalyzed by HPA-1 led to analogous results, in which the yield of carboxylic acids increased by almost a factor of two compared to that of the catalyzed reaction without *p*TSA (Table 4, entries 3 and 4). More precisely, the yield of carboxylic acids increased from over 10% to over 20%, while the yield of undesired by-products remained at a value of 19%. In addition, it was found that more AA than FA was formed with addition of *p*TSA compared to the reaction without addition of *p*TSA. Almost equal yields of about 5.5% for FA and AA were obtained without the addition of *p*TSA. In comparison, the addition of *p*TSA resulted in an AA yield of about 13% and a yield of FA of about 7%. Presumably, the use of *p*TSA as a solubilizer results in better accessibility of the humin to the catalyst, resulting in the C_2 product AA, while the reaction without *p*TSA mainly produces C_1 building blocks, which formed FA and also CO_2.

To exclude that *p*TSA acts as a source for carboxylic acids, the stability of this additive was tested under identical conditions but without the addition of substrate (Table 4, entry 5). The ^{1}H NMR spectra and HPLC chromatogram indicated no formation of carboxylic acids, as shown in the ESI† (Fig. S7 and S8). Furthermore, the results were confirmed using ^{13}C and 2D NMR. In addition, a stability experiment using the reduced form of the catalyst (HPA-1 blue) was conducted. For this purpose, the catalyst was completely reduced using oxalic acid. When completely reduced, the catalyst shows an intense blue color (see Fig. S9†). In ^{51}V NMR spectra, signals are no longer detectable due to the change of V^{5+} to V^{4+}, which is paramagnetic (see Fig. S9†). According to ^{1}H NMR (Fig. S10†) and HPLC (Fig. S11†), no carboxylic acids could be detected in the stability test using the fully reduced HPA-1 blue catalyst. Comparable results can also be found in the literature.[38]

Effect of *p*TSA concentration and reaction temperature on the SCO of humins

To further optimize the reaction, the influence of the amount of *p*TSA used and of the reaction temperature was also investigated in analogy to experiments using methanol. For this purpose, two further amounts of *p*TSA, 1.5 mmol and 6 mmol, were tested under otherwise identical reaction conditions. The results are shown in Table 5. The results show a linear dependence of the activity on the used amount of *p*TSA (Table 5, entries 2–4).

Table 4 SCO of humins using HPA-1 as catalyst and *p*TSA as solubilizer in aqueous phase

Entry[a]	Substrate	Catalyst	Additive	Total yield/%	Combined yield/%		Ratio[d] (value : waste)/%
					FA[b] + AA	CO + CO_2[c]	
1	Humin (Gl)	—	—	11.2	3.2	8.0	29 : 71
2	Humin (Gl)	—	*p*TSA	13.9	7.4	6.6	53 : 47
3	Humin (Gl)	HPA-1	—	30.1	10.9	19.2	36 : 64
4	Humin (Gl)	HPA-1	*p*TSA	39.1	20.1	19.0	51 : 49
5	—	HPA-1	*p*TSA	0.0	0.0	0.0	—

Experimental conditions: [a] 3-Fold reaction system, 90 °C, 30 bar O_2, 30 h, 1000 rpm, 300 mg solid humin (16.20 mmol carbon), 0.83 mmol of vanadium (V) for substitution (20 mol_{Carbon} mol_V^{-1}) and 3 mmol *p*TSA in 30 mL water. [b] Determined with quantitative ^{1}H NMR and *tert*-butanol as standard. [c] Determined with GC-TCD. [d] Calculated as described in corresponding section of the experimental part.

Table 5 SCO of humins using HPA-1 as catalyst and different amounts of *p*TSA

Entry[a]	Amount of *p*TSA/mmol	Total yield/%	Combined yield/%		Ratio[d] (value : waste)/%
			FA + AA[b]	CO + CO_2[c]	
1	0.0	30.1	10.9	19.2	36 : 64
2	1.5	49.9	23.7	26.2	47 : 53
3	3.0	39.1	20.1	19.0	51 : 49
4	6.0	33.1	15.7	17.4	47 : 53

Experimental conditions: [a] 3-Fold reaction system, 90 °C, 30 bar O_2, 30 h, 1000 rpm, 300 mg solid humin (16.20 mmol carbon), 0.83 mmol of vanadium (V) for substitution (20 mol_{Carbon} mol_V^{-1}) and 1.5–6.0 mmol *p*TSA in 30 mL water. [b] Determined with quantitative ^{1}H NMR and *tert*-butanol as standard. [c] Determined with GC-TCD. [d] Calculated as described in the corresponding section of the experimental part.

According to the results shown in Table 5, the total yield decreased from about 50% to about 33% when 1.5 mmol was used instead of 6.0 mmol, respectively. Therefore, the total yield decreased as the amount of *p*TSA increased. The influence of acid-induced effects and the polarity of the system could play a key role here, both increasing with a larger amount of *p*TSA. When adding more than 1.5 mmol *p*TSA, the pH of the solution drops significantly below pH 1 and thus leaves an adequate pH range, which could also negatively affect the results. This is also reflected in the combined yield of carboxylic acids, which reached its maximum at around 24% when 1.5 mmol *p*TSA was added (Table 5, entry 2). Based on the results, 1.5 mmol *p*TSA was considered as an optimum.

The reaction temperature can highly influence the kinetics of a reaction and thus the yield of carboxylic acids. To this end, experiments were conducted at different reaction temperatures using 1.5 mmol *p*TSA and the HPA-1 catalyst. The results are shown in Fig. 4. As expected, increasing the temperature from 90 °C to 120 °C also increased the total yield from about 50% to 94%. Unfortunately, the increase in activity mainly affected the yield of products in the gas phase, especially CO_2, which increased from around 26% at 90 °C to about 60% at 120 °C. This corresponds to an increase of a factor of 2.3, which is of a similar magnitude to the increase in total yield. Consequently, the increased activity primarily led to increased CO_2 formation through over-oxidation of the humin. In comparison, the combined yield of carboxylic acid increased only from about 24% to about 34% at 90 °C or 120 °C, respectively. Interestingly, most of this increase was achieved by increasing the reaction temperature from 90 °C to 100 °C, which increased the combined yield of carboxylic acids from about 24% to about 31%. A further increase in reaction temperature had only a minor influence on the combined yield of carboxylic acids and thus is insufficient. In summary, it can be concluded that the addition of *p*TSA as a solubilizer can significantly increase not only the activity but also the combined yield of carboxylic acids even at mild temperatures from 90 °C to 100 °C. Furthermore, the combined yields of carboxylic acid using *p*TSA at mild reaction temperatures could even compete with the yields using methanol at elevated reaction temperatures. However, the addition of *p*TSA did not inhibit CO_2 formation, therefore more undesired by-products than value-added products were formed. In particular, at higher temperatures, this effect was evident. In this regard, the addition of methanol was more beneficial compared to addition of *p*TSA. However, the combination of the effects of both additives could enable a new optimum in the SCO of humins.

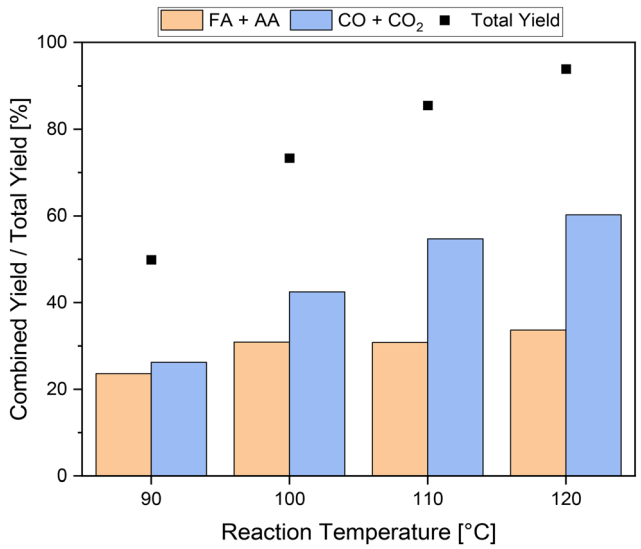

Fig. 4 SCO of humins using HPA-1 as catalyst at different reaction temperatures and *p*TSA as additive. Experimental conditions: 3-fold reaction system, 90–120 °C, 30 bar O_2, 30 h, 1000 rpm, 300 mg solid humin (16.20 mmol carbon), 0.83 mmol of vanadium (V) for substitution (20 mol_{Carbon} mol_V^{-1}) and 1.5 mmol *p*TSA in 30 mL water.

Optimization of the SCO of humins by synergetic combination of MeOH and *p*TSA as additives

In order to investigate whether the combination of solubilizer and alcoholic additive leads to synergetic effects, both 5 vol% methanol and 1.5 mmol *p*TSA were added to the reaction solution. The experiment was conducted at 120 °C, since at this reaction temperature the best results and a significantly increased activity were obtained in the experiments using methanol. Moreover, at 120 °C the efficiency of inhibition of CO_2 formation by methanol can be tested, since here the highest CO_2 yield was obtained in the experiments using *p*TSA. The results can be seen in Fig. 5. For comparison, the results for the individual additives at 120 °C are also shown.

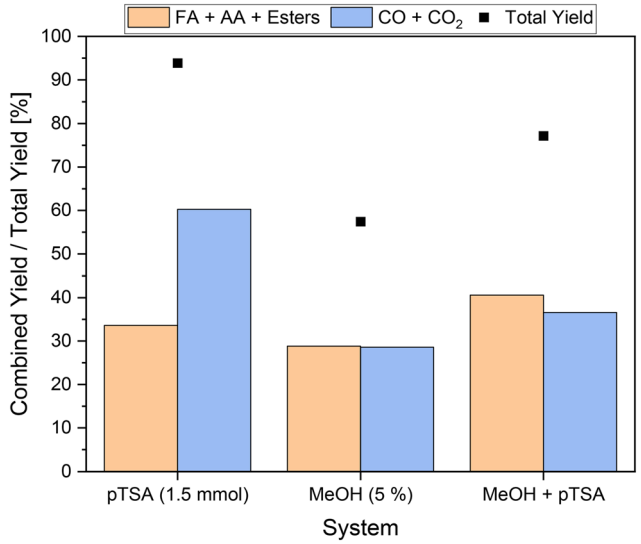

Fig. 5 SCO of humins using HPA-1 as catalyst in aqueous methanolic solution with *p*TSA (combined system). Experimental conditions: 3-fold reaction system, 120 °C, 30 bar O_2, 30 h, 1000 rpm, 300 mg solid humin (16.2 mmol carbon), 0.83 mmol of vanadium (V) for substitution (20 mol_{Carbon} mol_V^{-1}) in 5 vol% methanol with 1.5 mmol *p*TSA.

The results in Fig. 5 show that the total yield of the novel approach was intermediate between the total yields of the individual experiments. More specifically, a total yield of about 77% was achieved, which is almost equal to the average of 76% calculated form the results using the individual additives. This could be an indicator of additive interaction. On the one hand, *p*TSA as an additive increased the activity of the reaction. On the other hand, methanol inhibited CO_2 formation and thus slightly decreased the activity. This seems particularly plausible considering the combined yield of about 37% of undesired by-products, which is even below the average of 44% using the individual substrates. A combined yield of carboxylic acids of more than 40% was achieved, outperforming the yields obtained using the individual additives. As a result, more value-added products were produced than undesired by-products and significantly higher activity could be enabled.

In comparison to the pioneering experiments by Maerten *et al.*,[5] which so far represent the benchmark for the SCO of humins, the potential of the newly developed approach can be deduced. The yield of value-added products was increased by a remarkable factor of 3.6, while at the same time the yield of undesired by-products was 1.6 times lower. Three individual reactions were conducted as reproduction experiments to verify the results. It was possible to reproduce the results of liquid phase products with average yields of 26.0% ± 0.2%, 2.5% ± 0.1% and 12.1% ± 0.2% for FA, MF and AA, respectively. Average yields of 2.1% ± 0.1% and 32.8% ± 1.0% were reproduced for the gas phase products CO and CO_2, respectively. The results are found in the ESI† (see Fig. S12). In order to exclude the additives as the origin of carboxylic acids using the novel approach, stability tests were performed without the addition of substrate. According to NMR spectra and HPLC measurements, no carboxylic acids could be detected in the liquid phase after the reaction in these experiments. Furthermore, the formation of CO and CO_2 could not be confirmed by GC measurements.

Of further interest is the stability of the catalyst, as this also has a significant influence on the sustainability and economic effectiveness of the developed reaction system. A comparison of the ^{51}V NMR and ^{31}P NMR spectra of the catalyst before and after the reaction is helpful in this context. The vanadium-substituted POM catalysts can be analyzed structurally based on characteristic signals in the NMR spectra, which have already been discussed in detail in the literature.[24,39,45–49] Fig. 6 shows both the ^{51}V NMR spectra and the ^{31}P NMR spectra of the used

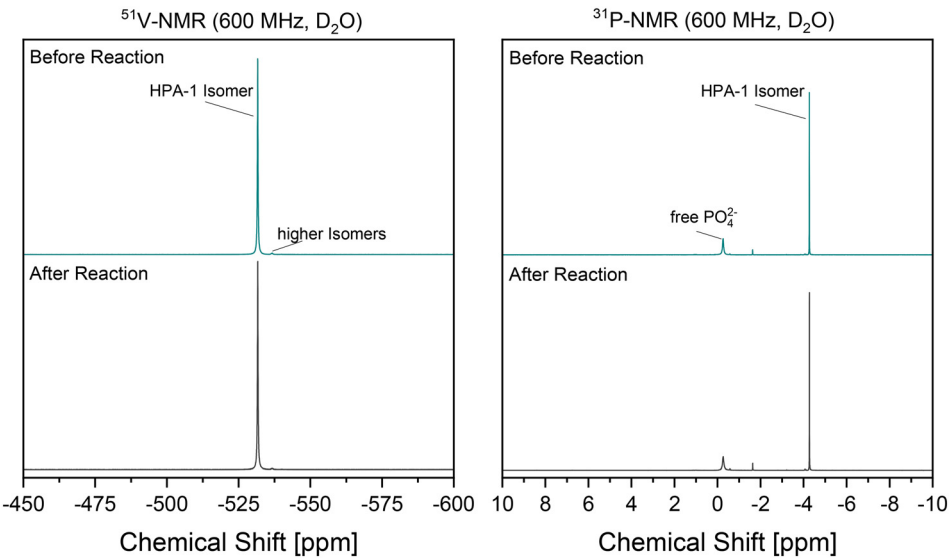

Fig. 6 Comparison of ^{51}V NMR (left) and ^{31}P NMR (right) spectra before and after the reaction. Experimental conditions: 3-fold reaction system, 120 °C, 30 bar O_2, 30 h, 1000 rpm, 300 mg solid humin (16.2 mmol carbon), 0.83 mmol of vanadium (V) for substitution (20 mol_{Carbon} mol_V^{-1}) in 5 vol% methanol with 1.5 mmol *p*TSA.

HPA-1 catalyst in the reaction solution. Due to the low degree of substitution, the spectra are extremely simple, as the number of possible isomers is restricted to almost one.

In addition, the formation of a complex mixture of isomers by dissociation and protolysis of higher substituted isomers is not possible, as these are practically non-existent using HPA-1. The comparison of the ^{51}V NMR spectra before and after the reaction reveal no changes. The signal at about −530 ppm, which can be assigned to the HPA-1 isomer, is retained. The same applies to the signal of the HPA-1 isomer at about −4.2 ppm in the ^{31}P NMR spectra. In particular, a strong increase in free phosphate (at −0.2 ppm) might indicate a decay of the Keggin structure, which was not observed. Overall, the results indicated that the structural integrity of the catalyst is given. In their study, Voß *et al.*[50] were able to demonstrate a continuous oxidation process in a comparable reaction system using a vanadium-substituted POM catalyst. Analogous to the experiments of Voß *et al.*,[50] a final evaluation of the catalyst stability and the associated preservation of catalytic activity in the reaction system developed here requires recycling experiments.

Initial investigations by Bertleff *et al.*[51] and previously published results[52] showed that efficient separation of the acidic oxidation products is essential for stable catalytic activity. In these studies, the decline in catalytic activity without separation of the acidic oxidation products could be attributed, among other things, to the formation of less substituted HPA isomers (HPA-1) at the expense of higher substituted isomers. This would not affect the present system since HPA-1 is already used, but a negative influence of catalysis cannot be ruled out if the oxidation products strongly accumulate. POMs are known to be extremely soluble in polar media, causing them to form a homogeneous phase with the product solution, making efficient separation difficult.[24,47,53] In this context, nanofiltration proved to be very promising, enabling rejections for the catalyst of over 99%, while carboxylic acids such as FA and AA were almost not rejected.[51,52]

To gain a deeper insight into the reaction process, the time-resolved reaction profiles were recorded and displayed in Fig. 7. For this purpose, individual reactions with reaction times of 0 h, 2 h, 4 h, 8 h, 16 h and 24 h were conducted and the liquid, gaseous and solid products were analyzed. In the first 4 h of reaction, the formation rate of the liquid phase and gas phase products was the highest and comparable to each other. Both achieved a combined yield of about 16% after 4 h. The amount of solid residue also decreased the strongest during this period. After 4 h, the formation of the products decreases significantly, although this effect is stronger for the gaseous products than for the liquid products. After 8 h, a combined yield of 24% and 20% was achieved for liquid products and gaseous products, respectively. In the subsequent reaction time up to 16 h and onwards, the combined yield of the carboxylic acids increased significantly more slowly, resulting in a very flattened course. The amount of solid residue also behaved similarly depending on the reaction time.

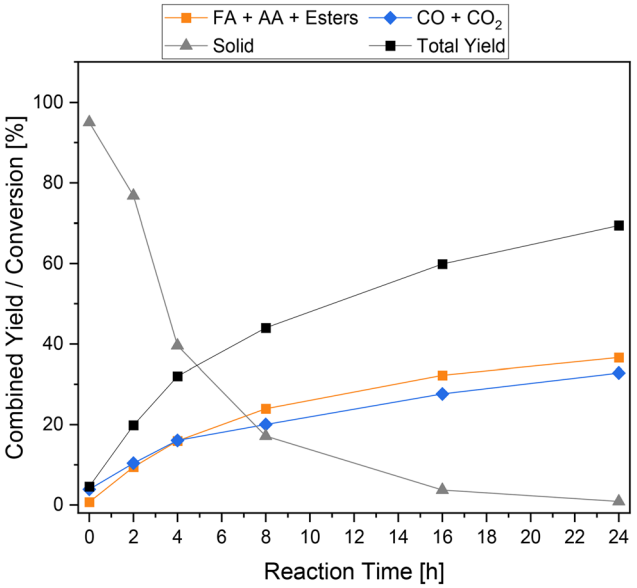

Fig. 7 Reaction course of the SCO of humins using HPA-1 as catalyst in aqueous methanolic solution with *p*TSA (combined system). Experimental conditions: 3-fold reaction system, 120 °C, 30 bar O_2, 0–30 h, 1000 rpm, 300 mg solid humin (16.20 mmol carbon), 0.83 mmol of vanadium (V) for substitution (20 mol_{Carbon} mol_V^{-1}) in 5 vol% methanol with 1.5 mmol *p*TSA.

Fig. 8 shows the results of the elemental analysis of the solid residue depending on the reaction time. Of particular interest are the mass fractions of oxygen (O) and carbon (C) and their ratio (O/C). In the first 4 h of reaction, the mass fraction of carbon decreased sharply from over 60% to below 50%, while the mass fraction of oxygen increased from about

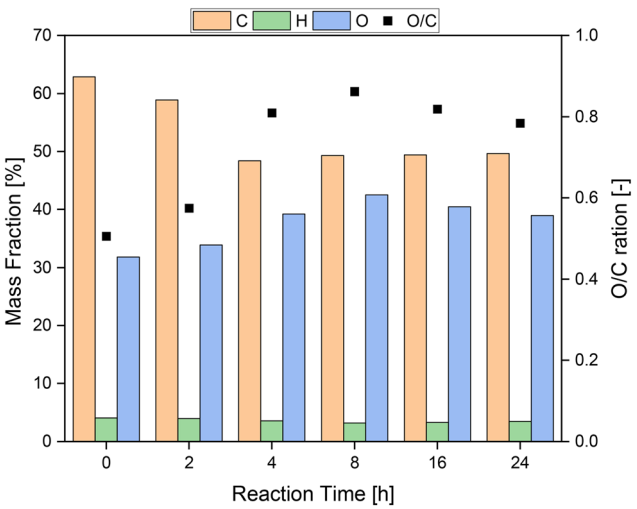

Fig. 8 Elemental analysis of residual humin from the SCO using HPA-1 as catalyst in aqueous methanolic solution with *p*TSA (combined system) depending on reaction time. Experimental conditions: 3-fold reaction system, 120 °C, 30 bar O_2, 0–24 h, 1000 rpm, 300 mg solid humin (16.20 mmol carbon), 0.83 mmol of vanadium (V) for substitution (20 mol_{Carbon} mol_V^{-1}) in 5 vol% methanol with 1.5 mmol *p*TSA.

30% to 40%. Hence, the oxygen–carbon ratio increased from about 0.35 to 0.80 in the first 4 h. Therefore, it seems plausible that functional groups were oxidized in the first hours of the reaction, but oxidative C–C bond cleavage also occurred, which induced oxygen-rich functional groups. After 8 h, the ratio of oxygen to carbon reached its peak with a value of almost 0.9. In the following hours the ratio fell slightly again, presumably because more oxygen was removed from the humin structure *via* the oxidation products than was introduced into the humin. This can also be recognized by the almost constant mass fraction of carbon after the first 8 h.

The solid residue was also analyzed by Fourier-transform infrared (FT-IR) spectroscopy to elucidate any structural changes in the humin depending on the reaction time. The results are shown in Fig. 9. Before catalysis, humin typical bands such as substituted furan rings (C=C, C–H vibration) could be observed at 1600 cm^{-1}, 1510 cm^{-1} and 1295 cm^{-1} and additional bands of carbonyl bonds at 1700 cm^{-1}.[9,21,27,54] During the course of the reaction, the bands corresponding to polysubstituted furan rings (1510 cm^{-1}), aldehydes and ethers (1090 cm^{-1}), and aliphatic chains (1295 cm^{-1}) decreased or disappeared completely.

In the first hours of the reaction, the band corresponding to carbonyl conjugated C=C double bonds (1600 cm^{-1}) became more intense. It can be assumed that the increase in the intensity of this bond is due to the oxidation of the insoluble humin residue and thus of alkyl groups or furan rings that could not be cleaved to form double bonds or ketones. Therefore, the number of double bonds conjugated to carbonyl compounds in humin would increase. The bands corresponding to C=O bonds (1710 cm^{-1}) in acids, aldehydes and ketones behaved in a similar manner. The increase in the mass fraction of oxygen measured by elemental analysis fits these observations. All these observations indicate that oxygen-functionalized bonds and groups were not only converted but also newly induced into the humin structure. Wassenberg *et al.*[21] described comparable observations in their study. In the range between 950 cm^{-1} and 1050 cm^{-1} new bands occurred, which most likely correspond to M=O bonds and P–O bonds of the catalyst.[24,55,56] At the end of the reaction, the intensity of all bonds decreased significantly.

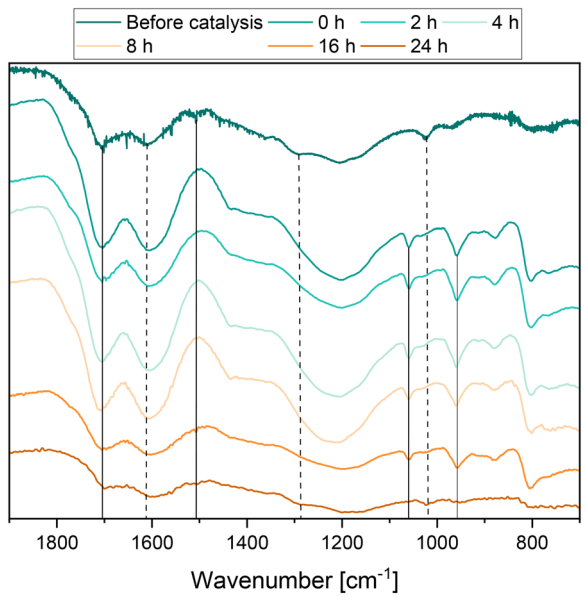

Fig. 9 IR spectra for the reaction course of the SCO of humin using HPA-1 as catalyst in aqueous methanolic solution with *p*TSA (combined system). Experimental conditions: 3-fold reaction system, 120 °C, 30 bar O_2, 0–24 h, 1000 rpm, 300 mg solid humin (16.20 mmol carbon), 0.83 mmol of vanadium (V) for substitution (20 mol_{Carbon} mol_V^{-1}) in 5 vol% methanol with 1.5 mmol *p*TSA.

Fig. 10 shows a hypothetical mechanism for the SCO of humins. Basically, the discussion of a mechanism is difficult, because despite extensive research, no reliable humin structure exists to date. However, as mentioned above, there are a number of plausible formation mechanisms and proven structural elements for humins, which have led to various models for its structure.[15–17,29,30,57] According to these models, the furan-rich network is predominantly cross-linked *via* aliphatic bonds and has numerous active oxygen functionalities. In the study by Zandvoort *et al.*,[29] 2D NMR spectra were used to demonstrate that the linkers are not simple methylene groups, but rather short aliphatic chains and oxygen-functionalized bonds forming structures similar to levulinic acid, for example. This seems plausible because the formation of humins is most probably based on the aldol condensation of the intermediates 5-HMF, DHH and levulinic acid.[17]

In the process, the formation of α,β-unsaturated carbonyl moieties or carbonyl moieties with hydroxy groups in the α-position is possible.[15,17,21,29] The humin model structure shown in Fig. 10 represents the combination of the various possible bonds and structures in one section. The fundamental framework is based on a model postulated by Filiciotto *et al.*[16] (Fig. 10, A), which was modified by a structural element confirmed by Wassenberg *et al.*[21] (Fig. 10, B) and a section according to Shen *et al.*[17] (Fig. 10, C).

Based on previously published results dealing with SCO of humin-like model substances, oxygen functionalization is essential for efficient conversion of the structures by POM catalysts.[23] The simplest types of oxygen functions are free functionalities such as aldehydes and carboxylic acids (Fig. 10, pathway 2). These functionalities can be converted directly by the catalyst. Here, an electron transfer (ET) to the catalyst occurs, which is consequently reduced ($V^V \rightarrow V^{IV}$). In this way, an oxidative C–C bond cleavage takes places at the carboxyl function with the elimination of CO_2. The oxidative C–C bond cleavage on the aldehyde follows a comparable mechanism. We assume that electron transfer is preceded by a nucleophilic attack of a water molecule in acidic medium, resulting in the elimination of FA. Previous publications have used this mechanism to accurately predict the yield of FA and CO_2 in the SCO of humin-like model substances, confirming the plausibility of this mechanism.[23] By eliminating a C_1 building block, a highly unstable furyl

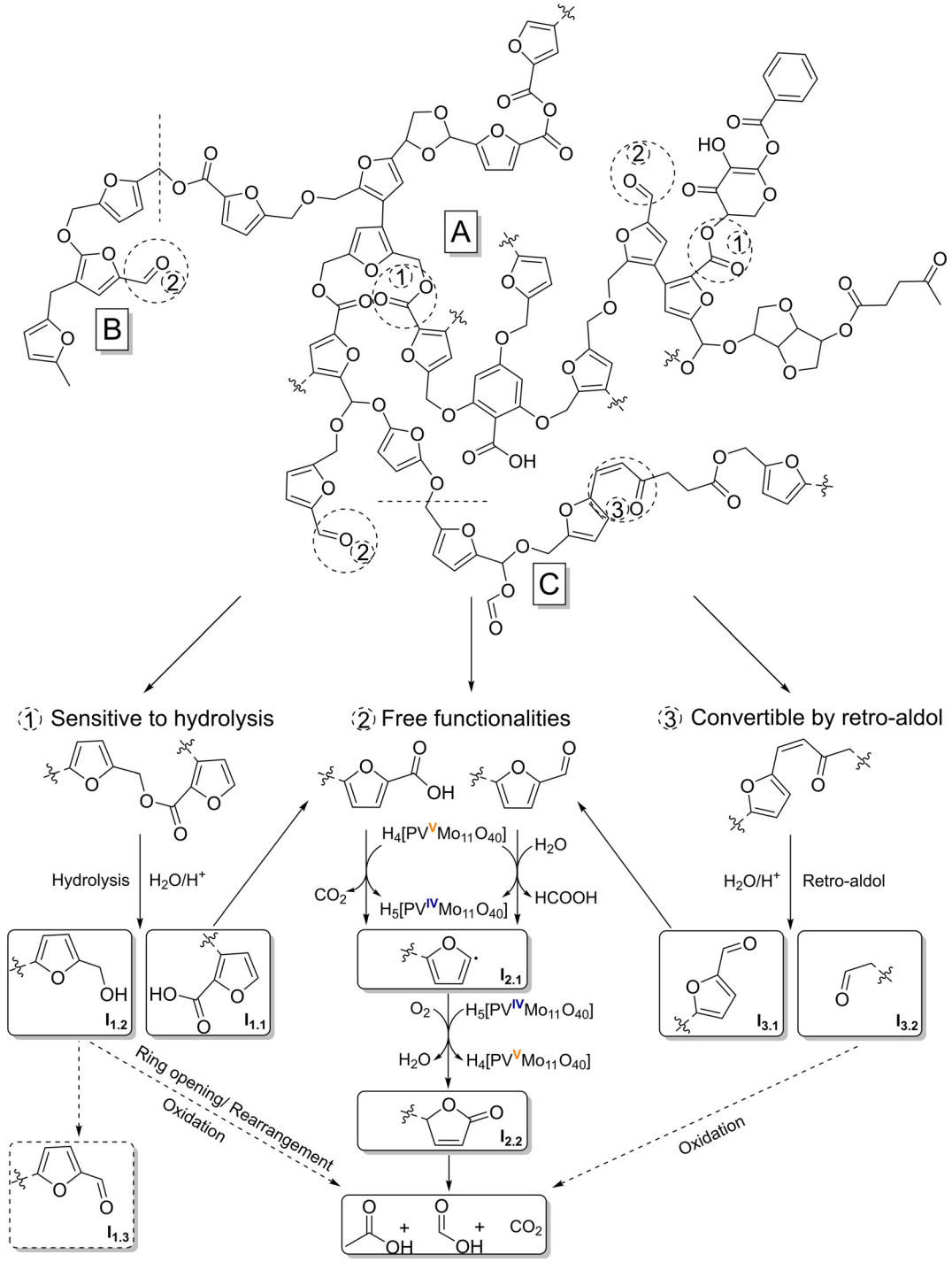

Fig. 10 Reaction mechanism for the selective catalytic oxidation of a modified humin model structure based on structural motifs published by Filiciotto *et al.*[16] (A), Wassenberg *et al.*[21] (B) and Shen *et al.*[17] (C) by converting humin typical functionalities that are hydrolysis-sensitive (1), free (2) or convertible by retro-aldol (3).

radical (Fig. 10, $I_{2.1}$) is formed, which is converted to a carbonyl function (Fig. 10, $I_{2.2}$) under the action of molecular oxygen and water. The catalyst is reoxidized during this process ($V^{IV} \rightarrow V^{V}$). Intermediate $I_{2.2}$ is structurally reminiscent of 2(5*H*)-furanone. In the experiments on the SCO of model substances, both 2(5*H*)-furanone and mainly 5-hydroxy-2(5*H*)-furanone as analogous compounds were detected.[23] Here the intermediate is still bound to the humin by a bond, therefore none of the intermediates could be detected in the reaction solution. The newly formed functionality opens new attack options as well as the possibility of ring opening. It has been demonstrated in previous studies on free furan systems that more strongly oxidized products such as maleic acid are formed as

subsequent products.[23] This is not possible in the present case because the ring system is still integrated into the humin structure, and thus additional C_1 and C_2 building blocks such as FA, AA and CO_2 are oxidatively eliminated. In this way, the humin structure is gradually broken down and new functionalization is repeatedly induced.

Another type of oxygen functionality are hydrolysis-sensitive bonds such as esters (Fig. 10, pathway 1). These bonds can be easily broken by acid catalysis, creating free functionalities ($I_{1.1}$) that can be converted according to pathway 2. Probably hydroxyl groups are also formed during the hydrolysis of esters ($I_{1.2}$). Under the prevailing oxidative conditions, the hydroxyl groups could oxidize to carbonyl moieties ($I_{1.3}$), which in turn can also be converted according to the described pathway 2. The oxidation of primary alcohols by POM catalysts has already been investigated and confirmed in the literature.[58–61] However, previous results on the free furan system in the form of furfuryl alcohol have shown that the intermediates 2(5*H*)-furanone and 5-hydroxyfuran-(25*H*)-furanone and the final product of this pathway (using free furan systems), maleic acid, were almost not formed.[23] Instead of maleic acid, products such as succinic acid and levulinic acid were detected, indicating a different mechanism.[23] It is known that furfuryl alcohol can rearrange in various ways and even hydrolytic ring openings are possible in aqueous solutions under acidic conditions.[62–67] Carbonyl moieties, γ-diketone, and conjugated diene structures as well as levulinic acid-like structures can form.[62–67] Oxidative ring opening is also feasible, leading to conjugated aldehydes.[67] These structures are more easily converted to short-chain products such AA, FA and CO_2 by the POM catalyst. This would be consistent with the SCO results for furfuryl alcohol.[23]

The α,β-unsaturated carbonyl moieties formed by aldol condensation can also be converted into more accessible structures by acid catalysis (Fig. 10, pathway 3). In a mechanism analogous to that of retro-aldol, these structures are cleaved by protonation of the carbonyl oxygen, nucleophilic attack of a water molecule in the β position and subsequent rearrangement. Comparable mechanisms have already been described in the literature for the SCO of cellulose using POM catalysts.[68] As a result, easy-to-convert carbonyl moieties near the furan ring ($I_{3.1}$) are created, which can be converted analogously to pathway 2. The formed aliphatic carbonyl moiety ($I_{3.2}$) should also be easy to convert, especially since it is usually close to other oxygen functionalities. This causes further C_1 and C_2 building blocks to be cleaved as AA, FA, and CO_2.

Overall, the mechanisms shown represent only a number of possibilities for the SCO of humins. These essentially depend on the actual humin structure, which is not yet completely elucidated. There are also structural models in the literature that stipulate a higher proportion of cross-linking *via* bonds without oxygen functionalization.[9,26,27,69,70] Ultimately, oxygen functionalization, albeit in lower proportions, enable oxidative degradation. Further mechanistic investigation of the reaction system for the SCO of humins and the integration of future insights on the structure elucidation of humins should be considered in further studies.

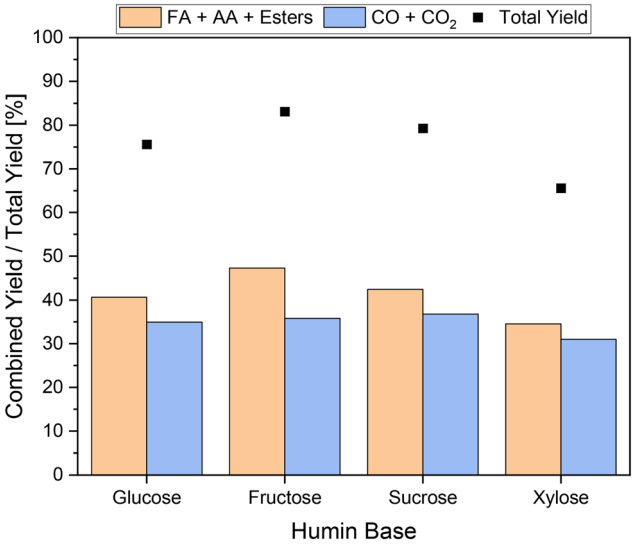

Fig. 11 SCO of various real humins using HPA-1 as catalyst in aqueous methanolic solution with *p*TSA (combined system). Experimental conditions: 3-fold reaction system, 120 °C, 30 bar O_2, 30 h, 1000 rpm, 300 mg solid humin (16.20 mmol carbon), 0.83 mmol of vanadium (V) for substitution (20 mol_{Carbon} mol_V^{-1}) in 5 vol% methanol with 1.5 mmol *p*TSA.

SCO of different real humins using the combined approach

In a final set of experiments, various real humins based on glucose, fructose, sucrose, and xylose were processed to verify the universal effectiveness of the newly developed approach. The results are shown in Fig. 11.

In all experiments, the combined yield of carboxylic acids exceeded the yields of undesired by-products. If a C_6-sugar was used as a substrate for humin synthesis, the yields of undesired by-products were at comparable values of around 36%. In the SCO of the fructose-based humin a combined yield of carboxylic acids of about 47% was achieved. The combined yield of carboxylic acids from the conversion of the sucrose-based humin was between those of glucose- and fructose-based humins. This seems plausible since sucrose is composed of glucose and fructose. Interestingly, the conversion of the xylose-based humin enabled the lowest total yield of only 66% and thus also the lowest combined yield of carboxylic acids below 35%. In contrast to hexoses, humin formation based on pentoses does not occur *via* 5-hydroxymethylfurfural (5-HMF) but *via* furfural; therefore fewer aldol condensations were involved in humin formation.[9,21] Moreover, the structure of xylose-based humin could be converted less efficiently. Nevertheless, it can be confirmed that the newly developed approach for the selective catalytic oxidation of humins is transferable to various humins and enables their efficient conversion to value-added products. Transferring the insights to higher substituted POM catalysts for the SCO of humins in the newly developed reaction system could be another interesting approach for system optimization. In this process, the use of additives could also help to prevent the over-oxidation of

humins caused by these much more active catalysts. This would allow a decrease in reaction temperature or reaction time, which could increase sustainability and economic viability. However, the question arises as to what extent the effects found are transferable and whether the additives are stable using higher substituted catalysts.

Conclusion

In the presented contribution we focused on the development of an optimized reaction system for the selective catalytic oxidation of water-insoluble and highly complex humins to short-chain carboxylic acid using Keggin-type polyoxometalates. We could demonstrate that a singly vanadium-substituted polyoxometalate catalyst exhibited a considerable selectivity advantage in the aqueous phase over higher substituted catalysts. More specifically, the yield of the undesired by-products CO and CO_2 was drastically decreased to a third, while the yield of carboxylic acids remained almost unchanged compared to that in benchmark experiments. Moreover, we applied alcohol additives with a remarkable inhibiting effect on CO_2 formation, further increasing the efficiency in the SCO of humins. As an alcohol additive, methanol in particular stands out due to the strongest inhibition of CO_2 formation compared to ethanol and isopropanol. For the first time, the oxidative valorization of humins produced more value-added products than undesired by-products such as CO_2. Furthermore, we investigated the influence of alcohol content and reaction temperature on the humin oxidation. It was shown that a temperature of 120 °C represents an optimum where methanol can still inhibit CO_2 formation even at a low alcohol content of 5 vol%. Due to these optimizations, the yield of carboxylic acids could be doubled without formation of CO_2 dominating. Furthermore, the use of *para*-toluenesulfonic acid (*p*TSA) as solubilizer has been investigated to circumvent the water-insoluble character of humins and thus optimize the activity. Using this solubilizer, the water-insoluble humin could be efficiently converted to equal yields of carboxylic acids and undesired by-products even without the CO_2-inhibiting effect of methanol. The activity of the reaction system was enhanced by optimizing the amount of solubilizer and the reaction temperature. However, the drastically increased activity led to a predominant formation of CO_2 and only to a small increase in value-added products. On the one hand, *p*TSA could efficiently promote the activity in oxidative valorization of humins. On the other hand, methanol was far more efficient in inhibiting CO_2 formation, especially at elevated reaction temperatures. Therefore, the combination of both additives at elevated reaction temperature was examined in a final optimization approach in order to exploit possible synergy effects. This novel approach enabled the highest yield of carboxylic acids and simultaneously the lowest yield of CO_2 reported to date in the SCO of humins. The results were reproducible and could even be transferred to various humins based on different sugars. We can conclude that using the combination of methanol and *p*TSA as additives as well as a singly vanadium-substituted polyoxometalate catalyst provides a highly promising approach in the selective catalytic oxidation of complex humins.

Experimental details

Chemicals

All chemicals were acquired commercially and used without further purification. To synthesize humins, acetic acid as an acid catalyst and various sugars were used. The sugars D(+)-glucose, D(−)-fructose, and D(+)-xylose (all for biochemistry) were purchased from Merck Millipore. Sucrose (99%) was obtained from Alfa Aesar. VWR Chemicals was the supplier of acetic acid (glacial).

For calibrations, reference spectra, and quantification, formic acid (97%) and *tert*-butanol (99%, ultrapure) obtained from VWR Chemicals and Grüssing were used.

For the presented study, singly V-substituted Keggin-type polyoxometalate catalyst, which can be described by the formula $H_4[PVMo_{11}O_{40}]$, was synthesis according to the literature.[23,39,71–73] In the selective catalytic oxidation of humins, additives were used to optimize the process. Alcohol additives were methanol (99.8%) and ethanol (99.8%) purchased from VWR Chemicals. As solubilizer, *p*TSA monohydrate (98%) obtained from Roth was used.

Catalyst characterization

To verify the stoichiometry of the synthesized $H_4[PVMo_{11}O_{40}]$ catalyst, inductively-coupled optical emission spectrometry (ICP-OES) was used. For the synthesized $H_4[PVMo_{11}O_{40}]$ catalyst, a stoichiometry of 1.23P/0.97V/11Mo was determined. Based on attenuated total reflection Fourier-transform infrared (ATR-FTIR) spectroscopy and ^{51}V as well as ^{31}P NMR spectroscopy, the integrity of the POM structure was verified. The results can be found in the ESI† (Fig. S13–S15).

Using a QATR™-S single-reflection ATR (with a diamond prism), the attenuated total reflection (ATR) FTIR spectrum of the catalyst was measured.

The respective service groups in the Department of Chemistry at Hamburg University conducted the following analyses:

Analysis of the catalyst to determine its stoichiometry was performed using a Fa. Spectro Arcos (Ametek) ICP-OES spectrometer. For the determination of the elemental composition (Mo, P, V) of the catalyst, it was dissolved in water (5 mL). Before measurement, 100 µL of a 65% aqueous nitric acid solution was added and subsequently diluted in a volumetric flask with water to 25 mL.

Nuclear magnetic resonance (NMR) measurements of the catalyst were conducted using a Bruker AVANCEII 600 MHz spectrometer. For the measurement, deionized water was acidified to pH 1 using a 37% aqueous hydrochloric acid solution in which 70 mg of catalyst was dissolved (0.7 mL). As the final preparation step, 0.07 mL of acetone-d6 was added. Measurements of the ^{31}P spectra were conducted in time domain (TD) data size of 32k, with a number of scans (NS) of 2k (=2048), a transmitter frequency offset for channel F1 (O1) and

a spectral width (SW) of −1 and 40 ppm. The settings of the aforementioned parameters for the measurements of the ^{51}V spectra were TD 32k, NS 4k, O1 and SW −520 ppm and 400 ppm and D1 0.5 s.

Experimental setup and general procedure of humin synthesis

Basically, the procedure described by Wassenberg *et al.*[21] was used for the synthesis of humins. To ensure a better reproducibility, larger batches of humin were prepared to perform oxidation experiments with the same batch. For this purpose, the humin synthesis was scaled up. A 600 mL autoclave made of Hastelloy (C-276) equipped with a gas entrainment impeller was used for the synthesis of large-scale humin batches. The synthesis was conducted under a nitrogen atmosphere, with acetic acid as acidic catalyst and a reaction time of 8 h. For the reaction, an aqueous acetic acid solution was prepared as a stock solution setting a pH value of 2. For this purpose, about 25 ml of acetic acid (glacial) were mixed with 200 ml of water. Subsequently, 36 g (0.2 mol) of glucose was weighed into a 400 mL glass liner and 200 mL of the acid solution was injected. This acid/solvent/sugar mixture provided a molar ratio of H^+/sugar of 1 : 100. The glass liner was inserted into the 600 mL autoclave, which was then sealed. To ensure a pure nitrogen atmosphere and to avoid oxidation reactions, the autoclave was purged three times with 45 bar nitrogen. Finally, a pre-pressure of 20 bar nitrogen was set. The reaction solution was stirred (300 rpm), the reaction temperature set to 180 °C, and the pressure increased to 45 bar. After 8 h of reaction, the heating jacket was turned off and removed. At a temperature below 30 °C, the autoclave was slowly ventilated and depressurized. The reaction solution containing the solid humin was filtered, rinsed with water, dried, and ground in a mortar. To ensure that no acid remains in the humin, the fine powder was cleaned with water using Soxhlet extraction for 24 h. The cleaned humin was dried for 24 h at 80 °C.

Experimental setup and general procedure of the SCO

For selective catalytic oxidation of synthesized humins a 3-fold reaction system was used. The plant has three identical 100 mL autoclaves made of stainless steel. Each autoclave was equipped with a heating jacket allowing reaction temperatures up to 200 °C, a gas entrainment impeller, and a 45 mL glass liner. All reactors were connected to an oxygen supply line.

In a typical experiment, each glass liner was filled with the appropriate amount of solid catalyst (0.83 mmol of vanadium), 300 mg humin (16.20 mmol carbon) and 30 mL of water. The filled glass liners were inserted into the autoclaves, and these were closed. To ensure a pure oxygen atmosphere, the closed autoclaves were purged three times with 30 bar oxygen. For experiments at a reaction temperature of 90 °C, the autoclaves were pressurized to a pre-pressure of 26.5 bar and the heating jackets were put on. Subsequently, the reaction temperature of 90 °C and a stirring speed of 300 rpm was set. When the desired reaction temperature inside the autoclaves was reached, the stirring speed was increased to 1000 rpm, which marked the start of the reaction. Due to the increase of temperature, the pressure increased to the desired value of 30 bar. At the end of each experiment, the temperature was set to 0 °C, the heating jackets were taken off and the stirring speed was decreased to 300 rpm, lowering the entrainment of oxygen into the liquid phase. When the temperature inside the autoclaves reached below 30 °C, samples of the gas phase could be taken. After venting the autoclaves, the glass liners were taken out of the autoclaves and the liquid phase was filtered.

In experiments using additives the experimental procedure was slightly adapted. The additive *p*TSA (0.285 g to 1.140 g (1.5 mmol to 6.0 mmol)) was filled into the glass liners in the form of its solid monohydrate. For experiments using alcohol additives, an aqueous solution of the respective alcohol as well as the desired alcohol content was prepared and charged into the glass liners instead of 30 mL water.

Analysis of substrates and reaction products

For quantitative measurement of the liquid phase, a Shimadzu HPLC system equipped with an HPX-87H 300 mm 7.8 mm Bio-Rad column and a refractive index detector was applied. An aqueous sulfuric acid solution at a concentration of 5 mmol L^{-1} was utilized as eluent. Measurements were conducted at a flow rate of 0.5 mL min^{-1}, a pressure of 49 bar, and a temperature of 45 °C.

A Varian 450-GC equipped with a TCD detector was used to measure the amounts of gaseous CO and CO_2.

FT-IR spectra of humins and the solid residue of the oxidation experiments were measured using the already mentioned (ATR) FT-IR device.

The respective service groups in the Department of Chemistry at Hamburg University conducted the following analyses:

A Model EA-3000 analyzer of Fa. EuroVector (Milano, Italy) was used for elemental analyses (CHNSO) of the synthesized humins and the solid residues after oxidation experiments.

NMR spectra of the reaction solutions were conducted using a Bruker AVANCEII 600 MHz spectrometer. The samples of the reaction solutions were prepared by blending 0.6 mL of the reaction solution with 0.1 mL of a 10 wt% *tert*-butanol solution in D_2O. The spectra were evaluated using the software MestReNova®.

Calculations

All calculated yields are based on the carbon provided by the substrate. When quantifying using ^1H NMR, a 10 wt% solution of *tert*-butanol as internal standard in D_2O was used. The molar amount n_{Proi} of a product i in the liquid phase can be calculated based on the ratio of its area A_{Proi} to the area A_{Stand} of the contained standard. The number of protons N_H that generate the signal must be taken into account, as shown in eqn (1). With the known molar amount n_{Stand} of standard in the sample and the mass of the sample, the mass fraction w_{Proi} of the respective substance can be calculated.

$$n_{\mathrm{Pro}i} = \frac{A_{\mathrm{Pro}i} \cdot N_{\mathrm{H,Stand}}}{A_{\mathrm{Stand}} \cdot N_{\mathrm{H,Pro}i}} \cdot n_{\mathrm{Stand}} \quad (1)$$

The yield $Y_{\mathrm{Pro}i}$ of a product i results from the ratio of its measured mass fraction $w_{\mathrm{Pro}i}$ to its theoretically possible mass fraction $w_{\mathrm{theo,Pro}i}$, as shown in eqn (2).

$$Y_{\mathrm{Pro}i} = \frac{w_{\mathrm{Pro}i}}{w_{\mathrm{theo,Pro}i}} \quad (2)$$

The theoretically possible mass fraction $w_{\mathrm{theo,Pro}i}$ is calculated by the ratio of the theoretically possible mass of a product i and the sum of the weights of the substrate m_{Sub}, pTSA $m_{p\mathrm{TSA}}$, catalyst m_{Cat} and solvent m_{Sol} (or alcohol-doped solution), as described in eqn (3). Here, the theoretically possible mass of a product i is calculated by the initial molar amount $n_{0,\mathrm{C}}$ of carbon provided by the substrate, the amount $N_{\mathrm{C,Pro}i}$ of carbon required for the formation of a product i and its molar mass $M_{\mathrm{Pro}i}$.

$$w_{\mathrm{theo,Pro}i} = \frac{n_{0,\mathrm{C}}/N_{\mathrm{C,Pro}i} \cdot M_{\mathrm{Pro}i}}{m_{\mathrm{Sub}} + m_{p\mathrm{TSA}} + m_{\mathrm{cat}} + m_{\mathrm{sol}}} \quad (3)$$

Based on the known mass fraction $w_{\mathrm{C,Sub}}$ of carbon in the substrate, the mass m_{Sub} of substrate and the molar mass M_{C} of carbon, the initial molar amount $n_{0,\mathrm{C}}$ of carbon was calculated, as described by eqn (4).

$$n_{0,\mathrm{C}} = \frac{w_{\mathrm{C,Sub}} \cdot m_{\mathrm{Sub}}}{M_{\mathrm{c}}} \quad (4)$$

Using eqn (5), the measured molar concentration of a product i $c_{\mathrm{Pro}i}$ was converted to the mass fraction of the product i $w_{\mathrm{Pro}i}$ for quantification by HPLC:

$$w_{\mathrm{Pro}i} = c_{\mathrm{Pro}i} \cdot \rho_{\mathrm{liq}} \cdot M_{\mathrm{Pro}i} \quad (5)$$

The yield could be calculated analogously to the quantification by NMR using eqn (2). The total yield is the sum of the yields of all products. Based on the total yield, the share of the value-added products (value) in the total yield was calculated according to eqn (6), taking into account the yields of the products formic acid Y_{FA}, methyl formate Y_{MF} and acetic acid Y_{AA}. The share of undesired by-products (waste) was calculated from the difference between 100 and the share of value-added products.

$$\mathrm{Value} = \frac{Y_{\mathrm{FA}} + Y_{\mathrm{MF}} + Y_{\mathrm{AA}}}{\sum_{0}^{i} Y_{\mathrm{Pro}i}} \times 100 \quad (6)$$

Conflicts of interest

There are no conflicts to declare.

Acknowledgements

J. A. and T. E. acknowledge financial support from the Deutsche Forschungsgemeinschaft (DFG) *via* the project AL 2130/5-1. Moreover, we thank the division for central element analytics, the division for NMR spectroscopy and the division for electron microscopy of the Department of Chemistry for conducting ICP as well as CHNS measurements, NMR experiments and SEM measurements, respectively. We also thank Jan-Christian Raabe for scientific support.

References

1 V. M. Chernyshev, O. A. Kravchenko and V. P. Ananikov, Conversion of plant biomass to furan derivatives and sustainable access to the new generation of polymers, functional materials and fuels, *Russ. Chem. Rev.*, 2017, **86**, 357–387.
2 Q. Hou, X. Qi, M. Zhen, H. Qian, Y. Nie, C. Bai, S. Zhang, X. Bai and M. Ju, Biorefinery roadmap based on catalytic production and upgrading 5-hydroxymethylfurfural, *Green Chem.*, 2021, **23**, 119–231.
3 K. H. Olsen, The clean development mechanism's contribution to sustainable development: a review of the literature, *Clim. Change*, 2007, **84**, 59–73.
4 V. P. Kashparova, D. V. Chernysheva, V. A. Klushin, V. E. Andreeva, O. A. Kravchenko and N. V. Smirnova, Furan monomers and polymers from renewable plant biomass, *Russ. Chem. Rev.*, 2021, **90**, 750–784.
5 S. G. Maerten, D. Voß, M. A. Liauw and J. Albert, Selective Catalytic Oxidation of Humins to Low-Chain Carboxylic Acids with Tailor-Made Polyoxometalate Catalysts, *ChemistrySelect*, 2017, **2**, 7296–7302.
6 J. J. Bozell and G. R. Petersen, Technology development for the production of biobased products from biorefinery carbohydrates—the US Department of Energy's "Top 10" revisited, *Green Chem.*, 2010, **12**, 539.
7 D. J. Hayes and M. H. B. Hayes, The role that lignocellulosic feedstocks and various biorefining technologies can play in meeting Ireland's biofuel targets, *Biofuels, Bioprod. Biorefin.*, 2009, **3**, 500–520.
8 K. Weissermel and H.-J. Arpe, *Industrial organic chemistry*, Wiley-VCH, Weinheim, 4th edn, 2003.
9 S. Liu, Y. Zhu, Y. Liao, H. Wang, Q. Liu, L. Ma and C. Wang, Advances in understanding the humins: Formation prevention and application, *Appl. Energy Combust. Sci.*, 2022, **10**, 100062.
10 S. K. R. Patil, J. Heltzel and C. R. F. Lund, Comparison of Structural Features of Humins Formed Catalytically from Glucose, Fructose, and 5-Hydroxymethylfurfuraldehyde, *Energy Fuels*, 2012, **26**, 5281–5293.
11 K. K. Kapanji, K. F. Haigh and J. F. Görgens, Techno-economics of lignocellulose biorefineries at South African sugar mills using the biofine process to co-produce levulinic acid, furfural and electricity along with gamma valeractone, *Biomass Bioenergy*, 2021, **146**, 106008.
12 M. J. Climent, A. Corma and S. Iborra, Conversion of biomass platform molecules into fuel additives and liquid hydrocarbon fuels, *Green Chem.*, 2014, **16**, 516.
13 G. Yang, E. A. Pidko and E. J. M. Hensen, Mechanism of Brønsted acid-catalyzed conversion of carbohydrates, *J. Catal.*, 2012, **295**, 122–132.

14 B. Girisuta, L. P. B. M. Janssen and H. J. Heeres, Kinetic Study on the Acid-Catalyzed Hydrolysis of Cellulose to Levulinic Acid, *Ind. Eng. Chem. Res.*, 2007, **46**, 1696–1708.

15 I. van Zandvoort, Y. Wang, C. B. Rasrendra, E. R. H. van Eck, P. C. A. Bruijnincx, H. J. Heeres and B. M. Weckhuysen, Formation, molecular structure, and morphology of humins in biomass conversion: influence of feedstock and processing conditions, *ChemSusChem*, 2013, **6**, 1745–1758.

16 L. Filiciotto, A. M. Balu, A. A. Romero, C. Angelici, J. C. van der Waal and R. Luque, Reconstruction of humins formation mechanism from decomposition products: A GC-MS study based on catalytic continuous flow depolymerizations, *Mol. Catal.*, 2019, **479**, 110564.

17 H. Shen, H. Shan and L. Liu, Evolution Process and Controlled Synthesis of Humins with 5-Hydroxymethylfurfural (HMF) as Model Molecule, *ChemSusChem*, 2020, **13**, 513–519.

18 B. Cheng, X. Wang, Q. Lin, X. Zhang, L. Meng, R.-C. Sun, F. Xin and J. Ren, New Understandings of the Relationship and Initial Formation Mechanism for Pseudo-lignin, Humins, and Acid-Induced Hydrothermal Carbon, *J. Agric. Food Chem.*, 2018, **66**, 11981–11989.

19 C. B. Rasrendra, M. Windt, Y. Wang, S. Adisasmito, I. G. B. N. Makertihartha, E. R. H. van Eck, D. Meier and H. J. Heeres, Experimental studies on the pyrolysis of humins from the acid-catalysed dehydration of C6-sugars, *J. Anal. Appl. Pyrolysis*, 2013, **104**, 299–307.

20 I. van Zandvoort, E. R. H. van Eck, P. de Peinder, H. J. Heeres, P. C. A. Bruijnincx and B. M. Weckhuysen, Full, Reactive Solubilization of Humin Byproducts by Alkaline Treatment and Characterization of the Alkali-Treated Humins Formed, *ACS Sustainable Chem. Eng.*, 2015, **3**, 533–543.

21 A. Wassenberg, T. Esser, M. J. Poller and J. Albert, Investigation of the Formation, Characterization, and Oxidative Catalytic Valorization of Humins, *Materials*, 2023, **16**(7), 2864.

22 J.-C. Raabe, T. Esser, F. Jameel, M. Stein, J. Albert and M. J. Poller, Study on the incorporation of various elements into the Keggin lacunary-type phosphomolybdate $[PMo_9O_{34}]^{9-}$ and subsequent purification of the polyoxometalates by nanofiltration, *Inorg. Chem. Front.*, 2023, **10**, 4854–4868.

23 T. Esser, A. Wassenberg, J.-C. Raabe, D. Voß and J. Albert, Catalytic Valorization of Humins by Selective Oxidation Using Transition-Metal-Substituted Keggin-Type Polyoxometalate Catalysts, *ACS Sustainable Chem. Eng.*, 2024, **12**(1), 543–560.

24 J.-C. Raabe, M. Poller, D. Voß and J. Albert, $H_8PV_5Mo_7O_{40}$ (HPA-5) - a unique polyoxometalate for acid and RedOx catalysis: synthesis, characterization, and modern applications in green chemical processes, *ChemSusChem*, 2023, e202300072.

25 M. J. Poller, S. Bönisch, B. Bertleff, J.-C. Raabe, A. Görling and J. Albert, Elucidating activating and deactivating effects of carboxylic acids on polyoxometalate-catalysed three-phase liquid–liquid-gas reactions, *Chem. Eng. Sci.*, 2022, **264**, 118143.

26 N. Shi, Q. Liu, R. Ju, X. He, Y. Zhang, S. Tang and L. Ma, Condensation of α-Carbonyl Aldehydes Leads to the Formation of Solid Humins during the Hydrothermal Degradation of Carbohydrates, *ACS Omega*, 2019, **4**, 7330–7343.

27 T. M. C. Hoang, E. R. H. van Eck, W. P. Bula, J. G. E. Gardeniers, L. Lefferts and K. Seshan, Humin based by-products from biomass processing as a potential carbonaceous source for synthesis gas production, *Green Chem.*, 2015, **17**, 959–972.

28 Z. Cheng, J. L. Everhart, G. Tsilomelekis, V. Nikolakis, B. Saha and D. G. Vlachos, Structural analysis of humins formed in the Brønsted acid catalyzed dehydration of fructose, *Green Chem.*, 2018, **20**, 997–1006.

29 I. van Zandvoort, E. J. Koers, M. Weingarth, P. C. A. Bruijnincx, M. Baldus and B. M. Weckhuysen, Structural characterization of ^{13}C-enriched humins and alkali-treated ^{13}C humins by 2D solid-state NMR, *Green Chem.*, 2015, **17**, 4383–4392.

30 H. Shan, L. Li, W. Bai and L. Liu, Evolution Process of Humins Derived from Glucose, *ChemistrySelect*, 2022, **7**(22), 7.

31 S. K. R. Patil and C. R. F. Lund, Formation and Growth of Humins via Aldol Addition and Condensation during Acid-Catalyzed Conversion of 5-Hydroxymethylfurfural, *Energy Fuels*, 2011, **25**, 4745–4755.

32 J. Horvat, B. Klaić, B. Metelko and V. Šunjić, Mechanism of levulinic acid formation, *Tetrahedron Lett.*, 1985, **26**, 2111–2114.

33 S. Wesinger, M. Mendt and J. Albert, Alcohol-Activated Vanadium-Containing Polyoxometalate Complexes in Homogeneous Glucose Oxidation Identified with ^{51}V-NMR and EPR Spectroscopy, *ChemCatChem*, 2021, **13**, 3662–3670.

34 T. Lu, Y. Hou, W. Wu, M. Niu, S. Ren, Z. Lin and V. K. Ramani, Catalytic oxidation of biomass to oxygenated chemicals with exceptionally high yields using H5PV2Mo10O40, *Fuel*, 2018, **216**, 572–578.

35 S. Maerten, C. Kumpidet, D. Voß, A. Bukowski, P. Wasserscheid and J. Albert, Glucose oxidation to formic acid and methyl formate in perfect selectivity, *Green Chem.*, 2020, **22**, 4311–4320.

36 Z. He, Y. Hou, H. Li, Y. Wang, S. Ren and W. Wu, Novel insights into CO_2 inhibition with additives in catalytic aerobic oxidation of biomass-derived carbohydrates to formic acid, *Renewable Energy*, 2023, **211**, 403–411.

37 Z. Tang, W. Deng, Y. Wang, E. Zhu, X. Wan, Q. Zhang and Y. Wang, Transformation of cellulose and its derived carbohydrates into formic and lactic acids catalyzed by vanadyl cations, *ChemSusChem*, 2014, **7**, 1557–1567.

38 J. Albert, R. Wölfel, A. Bösmann and P. Wasserscheid, Selective oxidation of complex, water-insoluble biomass to formic acid using additives as reaction accelerators, *Energy Environ. Sci.*, 2012, **5**, 7956.

39 J. Albert, D. Lüders, A. Bösmann, D. M. Guldi and P. Wasserscheid, Spectroscopic and electrochemical characterization of heteropoly acids for their optimized application in selective biomass oxidation to formic acid, *Green Chem.*, 2014, **16**, 226–237.

40 J. Albert, A. Jess, C. Kern, F. Pöhlmann, K. Glowienka and P. Wasserscheid, Formic Acid-Based Fischer–Tropsch Synthesis for Green Fuel Production from Wet Waste Biomass and Renewable Excess Energy, *ACS Sustainable Chem. Eng.*, 2016, **4**, 5078–5086.

41 J. Albert and P. Wasserscheid, Expanding the scope of biogenic substrates for the selective production of formic acid from water-insoluble and wet waste biomass, *Green Chem.*, 2015, **17**, 5164–5171.

42 P. Preuster and J. Albert, Biogenic Formic Acid as a Green Hydrogen Carrier, *Energy Technol.*, 2018, **6**, 501–509.

43 J. Reichert, B. Brunner, A. Jess, P. Wasserscheid and J. Albert, Biomass oxidation to formic acid in aqueous media using polyoxometalate catalysts – boosting FA selectivity by in-situ extraction, *Energy Environ. Sci.*, 2015, **8**, 2985–2990.

44 J. Reichert and J. Albert, Detailed Kinetic Investigations on the Selective Oxidation of Biomass to Formic Acid (OxFA Process) Using Model Substrates and Real Biomass, *ACS Sustainable Chem. Eng.*, 2017, **5**, 7383–7392.

45 J. Albert, M. Mendt, M. Mozer and D. Voß, Explaining the role of vanadium in homogeneous glucose transformation reactions using NMR and EPR spectroscopy, *Appl. Catal., A*, 2019, **570**, 262–270.

46 A. A. Shatalov, D. V. Evtugin and C. Pascoal Neto, Cellulose degradation in the reaction system O_2/heteropolyanions of series $[PMo_{(12\geq n)}V_nO_{40}]^{(3\leq n)-}$, *Carbohydr. Polym.*, 2000, 23–32.

47 V. F. Odyakov, E. G. Zhizhina, Y. A. Rodikova and L. L. Gogin, Mo-V-Phosphoric Heteropoly Acids and Their Salts: Aqueous Solution Preparation – Challenges and Perspectives, *Eur. J. Inorg. Chem.*, 2015, **2015**, 3618–3631.

48 L. Pettersson, I. Andersson, J. H. Grate and A. Selling, Multicomponent Polyanions. 46. Characterization of the Isomeric Keggin Decamolybdodivanadophosphate Ions In Aqueous Solution by 31P and 51V NMR, *Inorg. Chem.*, 1994, 982–993.

49 D. V. Evtugin, C. Pascoal Neto, J. Rocha and J. D. Pedrosa de Jesus, *Appl. Catal.*, 1981, **1**, 97–105.

50 D. Voß, M. Kahl and J. Albert, Continuous Production of Formic Acid from Biomass in a Three-Phase Liquid–Liquid–Gas Reaction Process, *ACS Sustainable Chem. Eng.*, 2020, **8**, 10444–10453.

51 B. Bertleff, R. Goebel, J. Claußnitzer, W. Korth, M. Skiborowski, P. Wasserscheid, A. Jess and J. Albert, Investigations on Catalyst Stability and Product Isolation in the Extractive Oxidative Desulfurization of Fuels Using Polyoxometalates and Molecular Oxygen, *ChemCatChem*, 2018, **10**, 4602–4609.

52 T. Esser, M. Huber, D. Voß and J. Albert, Development of an efficient downstream process for product separation and catalyst recycling of a homogeneous polyoxometalate catalyst by means of nanofiltration membranes and design of experiments, *Chem. Eng. Res. Des.*, 2022, **185**, 37–50.

53 N. I. Gumerova and A. Rompel, Polyoxometalates in solution: speciation under spotlight, *Chem. Soc. Rev.*, 2020, **49**, 7568–7601.

54 G. Tsilomelekis, M. J. Orella, Z. Lin, Z. Cheng, W. Zheng, V. Nikolakis and D. G. Vlachos, Molecular structure, morphology and growth mechanisms and rates of 5-hydroxymethyl furfural (HMF) derived humins, *Green Chem.*, 2016, **18**, 1983–1993.

55 J.-C. Raabe, J. Aceituno Cruz, J. Albert and M. J. Poller, Comparative Spectroscopic and Electrochemical Study of V(V)-Substituted Keggin-Type Phosphomolybdates and -Tungstates, *Inorganics*, 2023, **11**, 138.

56 J.-C. Raabe, J. Albert and M. J. Poller, Spectroscopic, Crystallographic, and Electrochemical Study of Different Manganese(II)-Substituted Keggin-Type Phosphomolybdates, *Chem. – Eur. J.*, 2022, **28**, e202201084.

57 X. Chen, N. Guigo, A. Pizzi, N. Sbirrazzuoli, B. Li, E. Fredon and C. Gerardin, Ambient Temperature Self-Blowing Tannin-Humins Biofoams, *Polymer*, 2020, **12**(11), 2732.

58 T. Wilke and M. A. Barteau, Dehydration and Oxidation of Alcohols by Supported Polyoxometalates: Effects of Mono- and Multivalent Cation Exchange on Catalyst Acidity and Activity, *Ind. Eng. Chem. Res.*, 2019, **58**, 14752–14760.

59 L. Jing, J. Shi, F. Zhang, Y. Zhong and W. Zhu, Polyoxometalate-Based Amphiphilic Catalysts for Selective Oxidation of Benzyl Alcohol with Hydrogen Peroxide under Organic Solvent-Free Conditions, *Ind. Eng. Chem. Res.*, 2013, **52**, 10095–10104.

60 A. M. Khenkin and R. Neumann, Oxidative C–C bond cleavage of primary alcohols and vicinal diols catalyzed by H5PV2Mo10O40 by an electron transfer and oxygen transfer reaction mechanism, *J. Am. Chem. Soc.*, 2008, **130**, 14474–14476.

61 A. Djaouida, M. Sadia and H. Smaïn, Direct Benzyl Alcohol and Benzaldehyde Synthesis from Toluene over Keggin-Type Polyoxometalates Catalysts: Kinetic and Mechanistic Studies, *J. Chem.*, 2019, **2019**, 1–11.

62 T. Kim, R. S. Assary, C. L. Marshall, D. J. Gosztola, L. A. Curtiss and P. C. Stair, Acid-Catalyzed Furfuryl Alcohol Polymerization: Characterizations of Molecular Structure and Thermodynamic Properties, *ChemCatChem*, 2011, **3**, 1451–1458.

63 L. Quinquet, P. Delliere and N. Guigo, Conditions to Control Furan Ring Opening during Furfuryl Alcohol Polymerization, *Molecules*, 2022, **27**(10), 3212.

64 M. Hronec, K. Fulajtárová and T. Soták, Kinetics of high temperature conversion of furfuryl alcohol in water, *J. Ind. Eng. Chem.*, 2014, **20**, 650–655.

65 G. M. González Maldonado, R. S. Assary, J. Dumesic and L. A. Curtiss, Experimental and theoretical studies of the acid-catalyzed conversion of furfuryl alcohol to levulinic acid in aqueous solution, *Energy Environ. Sci.*, 2012, **5**, 6981.

66 G. Falco, N. Guigo, L. Vincent and N. Sbirrazzuoli, Opening Furan for Tailoring Properties of Bio-based Poly(Furfuryl Alcohol) Thermoset, *ChemSusChem*, 2018, **11**, 1805–1812.

67 P. Delliere and N. Guigo, Revealed pathways of furan ring opening and surface crosslinking in biobased polyfurfuryl alcohol, *Eur. Polym. J.*, 2023, **187**, 111869.
68 J. Zhong, J. Pérez-Ramírez and N. Yan, Biomass valorisation over polyoxometalate-based catalysts, *Green Chem.*, 2021, **23**, 18–36.
69 S. Agarwal, D. van Es and H. J. Heeres, Catalytic pyrolysis of recalcitrant, insoluble humin byproducts from C6 sugar biorefineries, *J. Anal. Appl. Pyrolysis*, 2017, **123**, 134–143.
70 E. Licsandru, M. Gaysinski and A. Mija, Structural Insights of Humins/Epoxidized Linseed Oil/Hardener Terpolymerization, *Polymer*, 2020, **12**(7), 1583.
71 E. G. Zhizhina and V. Odyakov, Alteration of the physicochemical properties of catalysts based on aqueous solutions of Mo-V-P heteropoly acids in redox processes, *React. Kinet. Catal. Lett.*, 2008, **95**(2), 301–312.
72 E. G. Zhizhina, V. F. Odyakov and M. V. Simonova, Catalytic oxidation of organic compounds with oxygen in the presence of Mo-V-phosphoric heteropoly acid solutions, *Kinet. Catal.*, 2008, **49**, 773–781.
73 V. F. Odyakov and E. G. Zhizhina, A novel method of the synthesis of molybdovanadophosphoric heteropoly acid solutions, *React. Kinet. Catal. Lett.*, 2008, **95**, 21–28.